Spring 5-2015

# ENGINEERING OF LIPID NANOPARTICLES FOR ADVANCED DRUG DELIVERY APPLICATIONS

Stephen L. Hayward
*University of Nebraksa-Lincoln*, steh089@gmail.com

# ENGINEERING OF LIPID NANOPARTICLES FOR ADVANCED DRUG DELIVERY APPLICATIONS

by

Stephen L. Hayward

A THESIS

Presented to the Faculty of
The Graduate College at the University of Nebraska
In Partial Fulfillment of Requirements
For the Degree of Master of Science

Major: Chemical Engineering

Under the Supervision of Professor Srivatsan Kidambi

Lincoln, Nebraska
May, 2015

# ENGINEERING OF LIPID NANOPARTICLES FOR ADVANCED DRUG DELIVERY APPLICATIONS

Stephen L. Hayward, M.S.

University of Nebraska, 2015

Advisor: Srivatsan Kidambi

'Nanomedicine', the application of nanotechnology principles to the field of medicine, has stimulated the development of nano-platforms for next generation drug delivery. By exploiting nanoscale properties of materials to selectively alter intrinsic characteristics of therapeutics, researchers have improved the efficacy and pharmacokinetic profiles for a variety of drug types. Despite preliminary commercial and clinical success, there still remains a need to develop an improved delivery platform that can provide high cargo entrapment, efficient intracellular delivery, evasion of intracellular degradation pathways, and provide cell population specific targeting.

In this study we engineered a nanocarrier system composed of a core bilayer structure of biocompatible lipids and cholesterol, and an exterior surface coating of hyaluronic acid (HA). We optimized both the HA crosslinking reaction to the nanoparticle surface (HA-LNP), as well as the rehydration and entrapment conditions for optimal encapsulation efficiency. The HA-LNP system promoted uptake of an impermeable fluorescent model cargo as well as increased the therapeutic index of Doxorubicin by over 30 % compared to the free form counterpart. Confocal microscopy

was used to probe the endolysomal fate of HA-LNPs in cardiac, brain, and breast cells leading to validation of cell-dependent cytoplasmic distributions of the nanocarrier system with minimal lysosomal co-localization.

In order to investigate the effect of stiffness on nanoparticle uptake, we created 2D gel substrates with physiologically relevant stiffness ranging from 2kPa to 70 kPa. Flow cytometry was used to quantify HA-LNP uptake as a function of time and substrate stiffness in metastatic breast cancer cells. Interestingly we observed an initial preferential uptake mechanisms with cells on soft substrates both per cell and population wide, however at later time points we found that the overall capacity for HA-LNP uptake between all the substrates is equivalent, signifying the stiffness effect on HA-LNP uptake is transient. Further analysis of this mechanism could lead to the development of drug delivery platforms with increased intracellular delivery efficiency and specificity.

# AKNOWLEDGEMENTS

I would like to thank the multitude of people who have helped me complete this degree. First, I would like to thank my Fiancée, Joanna, for her seemingly boundless patience and unwavering support. I would also like to thank my father (Steve), mother (Michelle), and sister (Jacqueline) for always being there for me and instilling in me the principles of hard work and perseverance. I would also like to thank both sets of my grandparents for always looking out for me, teaching me important life lessons, and reminding me that life is about having fun and spending time with the ones you love. Furthermore, I would like to thank the Lorbers for putting up with my boring "advanced drug delivery" jargon and always making me feel at home. Lastly, I would like to thank the Piedmonts for continual life and academic guidance, as well as chicken parmesan to keep me going between visits back east.

I would also like to express gratitude to my advisor Dr. Srivatsan Kidambi for putting up with my occasionally stubborn demeanor as well as helping me become an independent researcher. His oversight, mentoring, spirited input, and financial/mental support made this project possible. I would also like to thank Dr. Velander and Dr. Saraf who are on my committee for their valuable input and helping shape this project. I am also grateful for the undergraduate researchers who has helped me on this project, especially David Francis, Matt Sis, and Parviz Kholmatov. Furthermore, I am also immensely grateful to my focus lab research cohort, Christina Wilson, Vaishaali Natarajan, and Amita Daverey, for making sure I go home at night and don't sleep in the lab. Finally I would like to thank the Department of Chemical and Biomolecular Engineering both for financial support as well as guidance in achieving this degree.

# TABLE OF CONTENTS

**CHAPTER 1 INTRODUCTION ..... 1**

1.1. Overview and Significance of Problem ..... 1

1.2. Background ..... 2

1.2.1. Need for Improved Nanoparticle Systems for Therapeutic Delivery ..... 2

1.2.2. Discovery of Liposomes ..... 2

1.2.3. Liposome Application in Drug Delivery ..... 3

1.3. Thesis Outline ..... 4

**CHAPTER 2: DEVELOPMENT OF A LIPID BASED NANOCARRIER SYSTEM CAPABLE OF HIGH ENTRAPMENT OF THERAPEUTIC CARGO ..... 5**

2.1. Introduction ..... 5

2.2. Materials and Methods ..... 7

2.2.1. Preparation of the LNPs ..... 7

2.2.2. Surface Modification of LNPs and the Lyophilization Process ..... 8

2.2.3. Entrapment protocol and Cargo Encapsulation Quantification ..... 8

2.2.4. Particle Size Distribution and Zeta Potential Analysis ..... 9

2.2.5. Transmission Electron Microscopy (TEM) ..... 9

2.3. Results and Discussion ..... 10

2.3.1. Lipid Nanoparticle System Characterization ..... 10

2.3.2. Nanoparticle Stability ..... 14

2.3.3. Analysis of Cargo entrapment (20, 70 kDa FD) and DOX ..... 14

2.3.4. TEM ..... 15

2.4. Conclusions ..... 15

**CHAPTER 3: INTRACELLULAR DELIVERY OF THERAPEUTICS TO CARDIAC, BRAIN, AND BREAST CELLS VIA THE LIPID NANOPARTICLE SYSTEM ..... 17**

3.1. Introduction ..... 17

3.2. Materials and Methods ..... 18

3.2.1. Cell Culture Protocol ..... 18

3.2.2. Therapeutic Cargo Uptake Experiments ..... 19

3.2.3. Flow Cytometry ..... 19

3.2.4. Confocal Microscopy ..... 20

3.2.5. Potency Assay ..... 20
3.2.6. Statistical Analysis ..... 21
3.3. Results and Discussion ..... 21
3.1.1. Naked vs HA-LNP encapsulated uptake of FD ..... 21
3.1.2. Potency Assay with DOX ..... 27
3.1.3. Endolysosomal Tracking of Fluorescently Tagged HA-LNPs ..... 30
3.4. Conclusions ..... 34
**CHAPTER 4: EFFECT OF SUBSTRATE STIFFNESS ON LIPID NANOPARTICLE UPTAKE ..... 35**
4.1. Introduction ..... 35
4.2. Materials and Methods ..... 36
4.2.1. PDMS Gel fabrication ..... 36
4.2.2. Gel Stiffness Characterization ..... 36
4.3. Results and Discussion ..... 37
4.3.1. Polymer Substrate Characterization ..... 37
4.3.2. Cell Morphology changes as a function of substrate stiffness ..... 38
4.3.3. Nanoparticle uptake as a function of stiffness ..... 40
4.4. Conclusions ..... 43
**CHAPTER 5: FUTURE WORKS ..... 44**
5.1. Targeted Nonviral Gene Delivery *in vitro* and *in vivo* ..... 44
5.2. Substrate Mediated Drug and Gene Delivery System ..... 45
5.3. Nanoparticle Biodistribution Analysis *in vivo* as a function of HA Length ..... 46
**References ..... 49**

# Table of Figures

**Figure 2. 1.** Lipid nanoparticle (LNP) fabrication overview schematic. .....11
**Figure 2. 2.** Optimization of the Hyaluronic Acid (HA) crosslinking reaction to the surface of the LNPs. Change in nanoparticle diameter (A) and surface charge (B) as a function of amide bond formation between the primary amine of the DPPE lipid and the carboxyl group of HA. .....11
**Figure 2. 3.** Particle Size distribution information of the nanoparticle systems. .....13
**Figure 2. 4.** Transmission Electron Microscopy (TEM) using the negative stain method with 2% phosphotungstic acid. Scale Bars are 250 nm for TEM. .....15

**Figure 3. 1.** Analysis of the cardiomyocyte (HL1) uptake of 20 and 70 kDa FD model drug in vitro. The model drug was utilized in two distinct forms: 1) encapsulated inside the aqueous core of HA-LNPs and 2) naked (no association with a nanocarrier). Plate reader quantification five hours post addition of the naked FD or HA-LNP-FD (*P<0.05, **P<0.005, ***P<0.0001; n=3). ..... 23
**Figure 3. 2.** Analysis of the cellular uptake of FD model drug to human breast cell lines in vitro. The model drug was utilized in two distinct forms: 1) encapsulated inside the aqueous core of HA-LNPs and 2) naked (no association with a nanocarrier). Plate reader quantification five hours post addition of the naked FD or HA-LNP-FD. (A) 20 kDa; (B) 70 kDa (*P<0.05, **P<0.005, ***P<0.0001; n=3). ..... 24
**Figure 3. 3.** Live confocal microscopy was used to validate the intracellular delivery of the 20kDa FD cargo from the HA-LNP-FD nanocarrier: A cluster of 21MT-1 breast cancer cells at 100x magnification with optical zoom (Scale bars are 5μm). ..... 25
**Figure 3. 4.** Live confocal microscopy was used to validate the intracellular delivery of the 70kDa FD cargo from the HA-LNP-FD nanocarrier: A cluster of 21MT-1 breast cancer cells at 100x magnification with optical zoom (Scale bars are 10μm). ..... 26
**Figure 3. 5** Analysis of the cellular uptake of fluorescently conjugated HA-LNPs to primary rat cerebellum astrocytes and a human glioblastoma cell line (A172). The fluorescent HA-LNPs were added, and analyzed for per cell fluorescent intensity via flow cytometry five hours post addition (*P<0.05, **P<0.005, ***P<0.0001; n=3). ..... 27
**Figure 3. 6.** Doxorubicin potency assay comparison between Free Dox and DOX encapsulated in HALNPs (HA-LNP-DOX). Standard MTT protocol was used to determine the % viable cells at 24 hours. ..... 28
**Figure 3. 7.** $LC_{50}$ nonlinear regression curves with both confidence and prediction bands for the 24 hr. potency assay comparison between the HA-LNP- DOX and free form DOX in 21MT-1 metastatic breast cancer cells..... 29
**Figure 3. 8.** Live confocal microscopy analysis of HA-LNP localization in the 21MT-1 metastatic breast cancer cell line in vitro. HA-LNPs with 0.15 mass % FITC tagged cholesterol in the lipid bilayer of the nanoparticles was used to track nanoparticle - endocytosis into the cell. (A) The cholesterol tagged HA-LNPs were incubated with the 21MT-1 cells for 5 hours and measured for co-localization with lysosomes to determine

the fraction of viable therapeutic that escapes the nanoparticle degradation pathway. (B) Confocal Microscopy with a Z-axis transformation of 21MT-1 cells at 100x zoom was used to validate cytoplasmic delivery by using the nucleus as a reference point inside the cell (The XZ plan shows the height and width of the cell). ..... 31
**Figure 3. 9.** Live confocal microscopy analysis of HA-LNP localization in the HL-1 mouse cardiomyocyte cell line in vitro. HA-LNPs with 0.15 mass % FITC tagged cholesterol in the lipid bilayer of the nanoparticles was used to track nanoparticle - endocytosis into the cell. The cholesterol tagged HA-LNPs were incubated with the HL-1 cells for 5 hours and measured for co-localization with lysosomes to determine the fraction of viable therapeutic that escapes the nanoparticle degradation pathway. ..... 32
**Figure 3. 10.** Live confocal microscopy analysis of HA-LNP localization in brain cells in vitro. HA-LNPs with 0.15 mass % FITC tagged cholesterol in the lipid bilayer of the nanoparticles was used to track nanoparticle - endocytosis into the cell. The cholesterol tagged HA-LNPs were incubated with the (A) A172 human glioblastoma cell line or (B) Primary rat cerebellum astrocytes for 5 hours and measured for co-localization with lysosomes to determine the fraction of viable therapeutic that escapes the nanoparticle degradation pathway. ..... 33

**Figure 4. 1.** Young's Modulus as a function of percent sylgard 184 polymer. This figure shows the tunability of the sylgard polymers to create and range of specific stiffness 2D gel substrates. .....38
**Figure 4. 2.** 21MT-1 metastatic breast cancer cells morphology depends on substrate stiffness. Confocal microscopy of fixed 21MT-1 cells atop (A) 2kpA, (B) 12.5 kPa, (C) 28 kPa, and (D) 70 kPa for 24 hours, followed by incubation with fluorescently tagged HA-LNPs for six hours. The blue is from the Hoescht nuclear stain. The scale bar is 50μm. .....39
**Figure 4. 3.** Flow Cytometry analysis of fluorescently conjugated HA-LNP uptake as a function of substrate stiffness: (A) Per cell fluorescent analysis and (B) % percent population FITC positive (*P<0.05, **P<0.005, ***P<0.0001; n=3, # denotes significance between the 2kPa and the sample marked following the same significance level designations as the stars). .....41

# Table of Tables

**Table 2. 1.** Dynamic Light Scattering, Electrokinetic Potential, and Drug Encapsulation Analysis of the Nanoparticle Systems. ..... 13
**Table 2. 2.** HA coated nanoparticle stability as a function of time. Stability was assessed by changes in particle diameter and surface charge. The HA-LNPs were stored in 4°C during the test. ..... 14

**Table 3. 1.** Potency assay summary ($LC_{50}$ values) between the free form DOX, and HA-LNP encapsulated DOX to 21MT-1 Metastatic Breast Cancer Cells at 24 hrs.....29

# CHAPTER 1 INTRODUCTION

## 1.1. Overview and Significance of Problem

The ability to control the spatial distribution and residence time profile of a therapeutic drug is a paramount goal and current hurdle for both biomedical engineering and the pharmaceutical sciences. In general, the vast majority of therapeutics utilized to treat a specific condition or ailment are employed in their "naked", non-altered, state. Since the human body is efficient at the identification and subsequent removal of foreign material, maximum tolerable doses commonly must be implemented in order to achieve an appreciable drug concentration at the site of interest. This mandatory high dosage regimen may ultimately lead to offsite toxic effects to various organ systems, induce potential host adaptation/resistance, restrict the types of drugs that can be used for therapeutic purposes, and impose a monetary burden for both drug research and development as well as treatment options for the consumer. In addition to high dosage concerns, naked administration of therapeutics is also limited in efficacy due to systemic attenuation, rapid clearance from the body, unfavorable intracellular delivery and population specificity, and potential for instigation of an immune response. Thus, there is a dramatic need for the development of novel methods and materials for the improvement in the transport of therapeutics cargo.

In order to address the limitations and potential toxicity of naked therapeutics, principles of nanotechnology have been applied to create novel platforms for next generation delivery systems. This hybrid field, termed Nanomedicine, exploits the nanoscale properties of materials to selectively alter the intrinsic characteristics of bare therapeutics such as solubility, diffusivity, half-life, biodistribution, and release kinetics

[1] to acquire enhanced drug pharmacokinetic profiles [2]. While Nanomedicine as a whole includes entities spanning from nanofibers to nanoscaffolds, nanoparticles have played a paramount role in advancing the nanoscale delivery of therapeutics. However, there is a need for the ability to deliver a range of different therapeutics with a single nanocarrier platform. The current single purpose- single nanoparticle platform ideology has greatly slowed the movement of robust drug delivery systems into both clinical trials and to market.

## 1.2. Background

### 1.2.1. Need for Improved Nanoparticle Systems for Therapeutic Delivery

Nanoparticle based drug delivery platforms operate on the same scale as biological systems, and therefore are ideal for the intracellular delivery of therapeutic cargo for the treatment of disease. To date, numerous drug delivery systems have been developed including gold nanoparticles [3], lipid vesicles [4], and protein based nanocarrier systems [5] amongst others. The central goal of these nanoparticle drug delivery systems is to capture, protect, and successfully deliver a therapeutic cargo to a specific coordinate in the body. However, there currently lacks a versatile, yet translatable, platform that can deliver a variety of therapeutic cargo types and sizes via a scale up friendly process for broad disease management.

### 1.2.2. Discovery of Liposomes

Liposomes are spherical vesicles of ~100 nm diameter consisting of a lipid bilayer shell and an aqueous core held together by amphipathic molecule driven stabilization. This structure was discovered by Alec Bangham and coworkers in the mid-1960s [6, 7], and has since been the standard model system for biological membranes [8]. Liposomes

are comprised principally from phospholipids and cholesterol, but can also obtain other components with favorable amphipathic properties. Upon contact with water, lipid molecules will self-assemble into three dimensional structures as a function of thermodynamics, interaction free energies, and geometry between the polar head group and nonpolar tail (s) [9]. Many methods have been studied to create monodisperse populations of liposomes including agitation (sonication), mechanical extrusion, solvent dispersion, and detergent removal [10]. The precise method that should be used is dependent upon the final application of the particles, the physicochemical properties of the specific lipids, and the potential for scale up.

### 1.2.3. **Liposome Application in Drug Delivery**

Liposomes are extremely versatile nanocarriers that have been studied and utilized extensively for drug delivery applications due to their ease of creation, large protective hydrophilic inner cavity for encapsulation, and controllable drug release kinetics. As a result of unique bilayer structure, liposomes are able to efficiently encapsulate and improve the pharmacokinetics of both hydrophobic and hydrophilic cargo. Furthermore, liposomes can be tailored for specific applications by either structural based changes such as overall particle size and extent of membrane fluidity, and also by altering their surface characteristics such as charge, steric effect (hydration), and targeting potential. This high degree of freedom of exterior customization has been utilized to create long circulating "stealth" liposomes [11], as well as liposomes that can target specific cell populations via active targeting means [12-15].

Currently, over 15 liposome and lipid based drug formulations are approved for clinical use, with over 600 additional clinical trials in progress [11, 16-18]. These

formulations span treatment areas ranging from cancer and preventive vaccination to microbes and hormone replacement. However, each of these delivery formulations is constrained to a specific cargo type and subsequently a pre-determined function. Consequently, there remains a need for a lipid based platform capable of delivery of a variety of cargo types with high encapsulation, favorable intracellular delivery, and potential for industrial scale up to catalyze the commercialization of next generation drug delivery systems.

## 1.3. Thesis Outline

This thesis focuses on developing a lipid nanoparticle system for advanced drug delivery applications and is subdivided as follows: Chapter 2 described the optimization steps in nanoparticle fabrication and optimal cargo entrapment. In addition, Chapter 2 goes over through characterization of the nanocarrier system and also tests the overall stability of the particles. Chapter 3 probes the potential of the nanocarrier system to undergo efficient intracellular delivery. Specifically, Chapter 3 investigates the delivery of a range of different model therapeutics in breast, brain, and cardiac cells. Chapter 3 also probes the endolysosomal fate of the nanocarrier system in all three cell types. Chapter 4 describes the investigation of the effect of substrate stiffness on nanoparticle uptake in cancer cells, and discusses how this information can be used to create next generation drug delivery systems with increased population targeting specificity. Chapter 5 concludes the thesis with goals and suggestions for future work with the aforementioned nanocarrier system.

# CHAPTER 2: DEVELOPMENT OF A LIPID BASED NANOCARRIER SYSTEM CAPABLE OF HIGH ENTRAPMENT OF THERAPEUTIC CARGO

## 2.1. Introduction

The ambition to safely and reproducibly transport a therapeutic cargo to a specific coordinate of the body is a main catalyst for the development of next generation advanced drug delivery systems. Both bare and surface functionalized liposomes, termed lipid nanoparticles (LNPs), have been used to successfully circumvent non-ideal characteristics of therapeutic drugs leading to 1) significant improvement in half-life *in vivo* and 2) reduction in systemic toxicity prompting potent improvement in therapeutic index [19, 20]. However, the initial step of cargo entrapment has remained a main hurdle for the implementation of lipid based drug delivery systems.

In order to successfully deliver a hydrophilic drug, liposomes must first encapsulate the cargo into either the aqueous interior of the nanoparticle. This entrapment procedure can be performed either passively, during liposome formation, or actively, post liposome formation. Passive entrapment of hydrophilic cargo requires addition of the drug into the rehydration medium of the initial dry lipid film encouraging entrapment during primary vesicle formation. This procedure leads to low entrapment efficiencies due to the small internal volumes of the nanoparticles as compared to the bulk solution [21]. In addition, since the drug is introduced early in the liposome formation process, appreciable drug degradation is possible during subsequent processing steps.

Active mechanisms for hydrophilic drug loading into liposomes includes pH gradient loading [22], temporary liposome and/or drug permeabilization [23], and the

lyophilization and rehydration method [24-27]. While all three active loading approaches lead to drug entrapment post liposome formation, the lyophilization and rehydration technique has many advantages over the other two methods. The lyophilization and rehydration method involves forming liposomes in drug-free physiological buffers, followed by a quick snap freeze and a subsequent highly controlled freeze dry step to achieve a dry lipid film. During this freeze dry process the liposome is gently lowered out of solution and when the driving force for self-assembly is critically reduced, the nanoparticle will open up into a lipid bilayer sheet and adhere to the bottom of the container. Upon careful rehydration, the dry lipid film will swell and spontaneously re-form into a liposome via interaction with and entrapment of local solution. By adding drug into this rehydration medium, high drug entrapment has been achieved [26, 28].

A significant hurdle for widespread implementation of the lyophilization and rehydration procedure is vesicle fusion upon rehydration. Without a lyoprotectant added to the liposome containing solution prior to snap freezing, such as the disaccharide trehalose, appreciable vesicle fusion occurs during the rehydration step yielding micro scale particles impractical for drug delivery purposes. To evade the use of free sugar molecules, the synthetic polymer polyethylene glycol (PEG) [29] or naturally derived extracellular matrix protein such as hyaluronic acid (HA) [30-33] have been covalently cross linked to the liposome surface prior to lyophilization to act as steric barriers during the rehydration step. However, there is currently a need to develop an actively loaded liposome delivery system capable of efficient entrapment of a range of therapeutic sizes and long term stability in solution with a potential for scale up.

Herein, we have engineered a lipid nanoparticle system comprised of a core structure of biocompatible lipids and cholesterol, and a surface decorate of high MW HA. We optimized both the HA crosslinking reaction to the nanoparticle surface, as well as the rehydration and entrapment conditions for optimal entrapment efficiency. We modeled a range of therapeutic entrapment by utilizing the fluorescently tagged model drugs: 1) 20 kDa FITC tagged Dextran (20 kDa FD) – model drug for silencing RNA entrapment, 2) 70 kDa FITC tagged Dextran (70 kDa FD) – model drug for protein based therapeutics, and 3) Doxorubicin (DOX) – model drug for small molecule inhibitors and chemotherapeutics.

## 2.2.Materials and Methods

### 2.2.1. **Preparation of the LNPs**

Multilamellar vesicles (MLV) composed of L α-Phosphatidylcholine (PC) (Avanti Polar Lipids), 1, 2- Dipalmitoyl-sn-Glycero-3-Phopshoethanolamine (DPPE), and Cholesterol (CHOL) (both from Sigma Aldrich) were created via the traditional dry film method as previously reported [14, 28, 30, 31, 33, 34]. This MLV solution was allowed to rest overnight at 4°C, and the next day was mechanically extruded using an Mini Extruder Apparatus (Avanti Polar Lipids) maintained at 65-70 °C in a stepwise fashion with progressively smaller membrane pore sizes to reach a final unilamellar vesicle (ULV) in the size range of 80-100 nm hydrodynamic diameter. Each membrane size underwent numerous cycles to ensure final product homogeneity.

### 2.2.2. **Surface Modification of LNPs with Hyaluronic Acid and the Lyophilization Process**

Hyaluronic Acid (HA), ~1.65 MDa (Sigma) was dissolved in Sodium Acetate Buffer (pH 5) to a final concentration of 2 mg/ml. The HA was activated in solution with 1-ethyl-3-(3-dimethylaminopropyl) carbomiide (EDAC) (Sigma) at a mass ratio of 1:20 respectively via gentle mixing at 37°C (pH ~4) for 2 hours [35]. The post extrusion LNPs were separated from lipid debris by ultracentrifugation (140,000 g, 4°C, 1.5 hr.) followed by rehydrating the pellet in 0.1M Borate Buffer (pH 8.6). The activated HA solution was combined with the purified LNP solution and incubated for 24 hours at 37°C (pH 8.6) with gentle mixing to mediate amide bond formation. Separation of the resulting HA-LNP from excess reagents in solution was achieved by washing three times using ultracentrifugation. Following purification, the particles were aliquoted, snap frozen, and lyophilized for 60 hrs. using a Chamber Freeze Dry System (Labconco) [31]. The lyophilized particles were stored at -80 °C until use.

### 2.2.3. **Rehydration (Entrapment) protocol and Cargo Encapsulation Quantification**

The lyophilized HA-LNP particles were rehydrated with $1/10^{th}$ of the original solute volume composed of nuclease free water containing the cargo (FITC-Dextran or Doxorubicin), followed by quick vortex agitation to ensure the full quantity of lyophilized powder was hydrated. After total rehydration the mixture was left to rest for 30 minutes to allow for lipid membrane re-assembly. Following this rest period, PBS solution was added to the sample to match the initial pre-lyophilization volume and un-encapsulated drug was removed by ultracentrifugation (140,000 g, 4°C, and 1.25 hr.). For

encapsulation efficiency determination of the FITC tagged Dextran (FD) (Sigma) cargo, fluorescence at 495 nm em/ 520 em was measured in the presence of 0.1 % Triton X-100 detergent to disrupt the lipid bilayers. With a known amount of fluorescent drug present during the entrapment procedure, a standard curve was utilized to determine the amount entrapped. The analogous procedure was performed to determine the encapsulation efficiency of Doxorubicin (Sigma) using the natural fluorescence of the chemotherapeutic (ex. 470 nm, em. 585 nm).

#### 2.2.4. **Particle Size Distribution, Hydrodynamic Diameter, and Zeta Potential Analysis**

Particle size distribution, mean diameter, and zeta potential were measured using a NanoBrook ZetaPALS zeta potential and dynamic light scattering instrument (Brookhaven). The particle size distribution and mean hydrodynamic diameter was analyzed as both intensity and volume averaged distributions using a scattering angle of 90°. The Smoluchowki model was utilized to calculate the zeta potential from mobility measurements. All measurements were performed in 0.05x PBS (pH 7.4) at 25 deg C.

#### 2.2.5. **Transmission Electron Microscopy (TEM)**

The phosphotungstic negative stain method was utilized for visualization of the LNP system. A drop of each sample (HA-LNP, HA-LNP-70 kDa FD, LNP Pre-Lyophilization, and LNP Post-Lyophilization) was applied to separate copper grids coated with a carbon film and left to air dry. A 2% phosphotungstic acid solution was applied for negative staining, and the samples were analyzed in the UNL Microscopy Core Research Facility's TEM (Hitachi H7500).

## 2.3.Results and Discussion

### 2.3.1. **Lipid Nanoparticle System Characterization**

To develop a nanocarrier system capable of high cargo entrapment efficiency for a range of therapeutic sizes and long term stability in solution, we first engineered highly customizable LNPs as described in **Fig 2.1**. The LNPs were composed of the natural/ biocompatible lipids PC and DPPE in combination with cholesterol, and had a mean particle size of 93.6 ± 0.4 nm, a polydispersity index of 0.061, and a slightly negative surface charge of -9.46 ± 0.31 mV as measured by DLS and a Zeta Potential Analyzer. To successfully surface decorate the LNPs with high MW Hyaluronic Acid (HA), crosslinking optimization between the primary amine of DPPE and the carboxyl group of HA was performed to ensure effective surface functionalization under conditions that limit the formation of large aggregate structures (**Fig 2.2**). Specifically, a ratio of 65 μg HA/ μmole lipid during the reaction procedure was found to be the ideal condition for single nanoparticle-HA amide bond construction, leading to the formation of a monodisperse population of HA coated LNPs. Following this DPPE-HA crosslinking procedure, the mean particle size increased to 157.2 ± 1.2 nm, a polydispersity index of 0.105, and a moderately negative surface charge of -38.07 ± 0.35 mV due to the presence of HA's charged carboxyl groups.

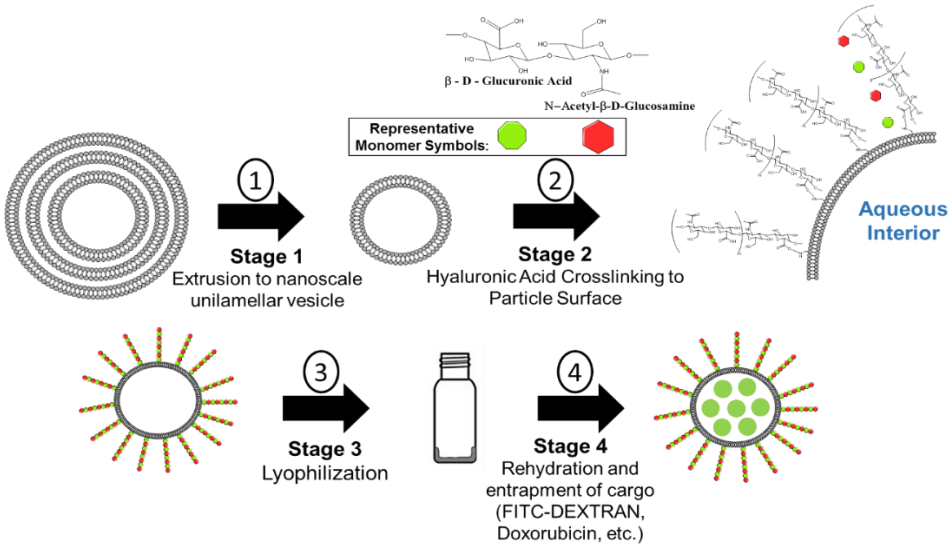


**Figure 2. 1.** Lipid nanoparticle (LNP) fabrication overview schematic.

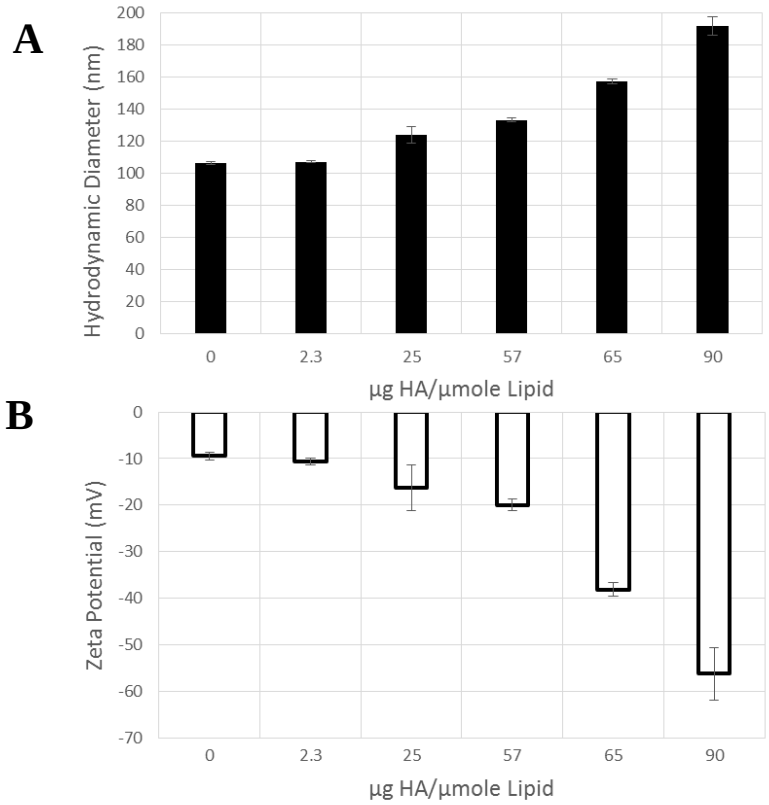


**Figure 2. 2.** Optimization of the Hyaluronic Acid (HA) crosslinking reaction to the surface of the LNPs. Change in nanoparticle diameter (A) and surface charge (B) as a

function of amide bond formation between the primary amine of the DPPE lipid and the carboxyl group of HA.

Following the lyophilization process and subsequent rehydration in the presence of physiological buffer, the HA-LNPs particle size increased minimally and underwent no significant change in net surface charge indicating that all HA remained on the outside of each particle during the bilayer reformation process. This step was crucial to ensure that the HA-LNPs would not be structurally altered during the entrapment procedure.

Next, we wanted to study the rehydration of the HA-LNPs in the presence of a model drug molecule, FITC-tagged Dextran (FD), to optimize drug entrapment conditions. A range of molecular weight FD (10, 20, and 70 kDa) was successfully encapsulated and used to demonstrate that the diameter of the HA-LNP carrier post drug entrapment is not a function of the size of the cargo in the aqueous interior of the nanoparticle, as well as the versatility of the carrier to entrap a broad range of cargo sizes. The chemotherapeutic Doxorubicin (DOX) was also successfully encapsulated in an analogous manner with additional precautions taken to avert degradation. Comprehensive data on particle size, surface charge, and cargo entrapment is located in **Table 2.1**. Particle size distributions of the nanoparticle systems HA-LNP, HA-LNP-FD (10, 20, and 70 kDa), and HA-LNP-DOX were also probed to confirm that in each case a monodisperse population of particles was obtained **(Fig 2.3)**.

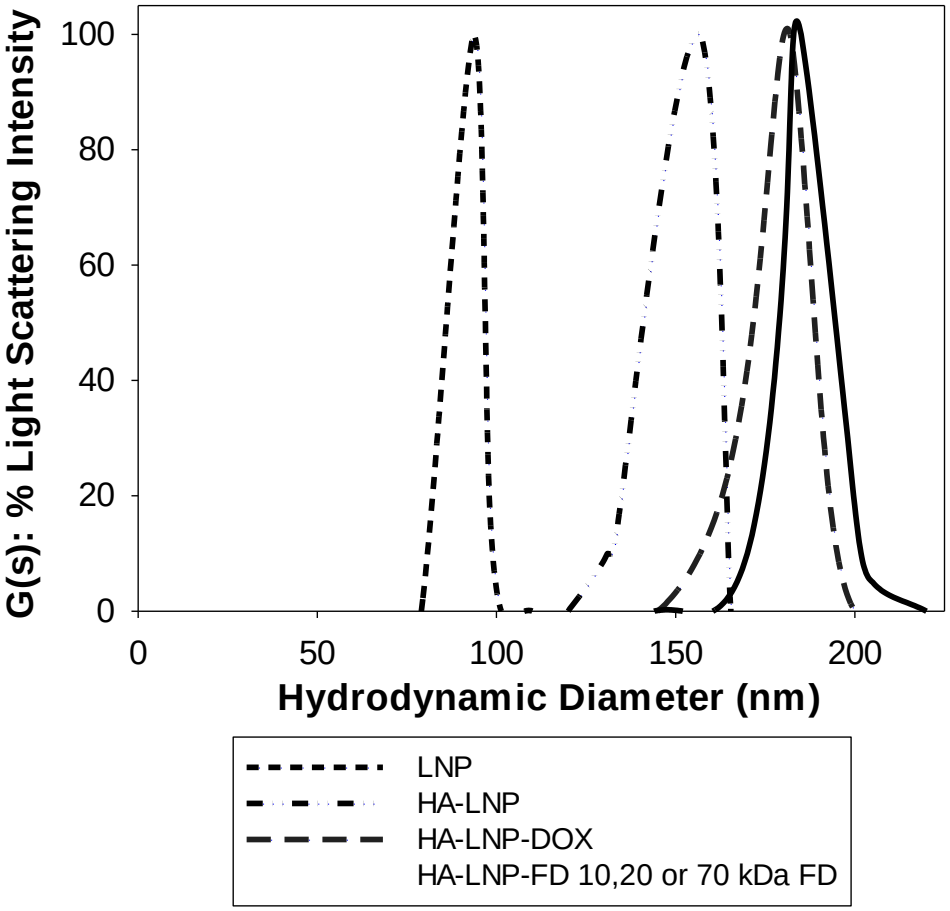


**Figure 2. 3.** Particle Size distribution information of the nanoparticle systems.

**Table 2. 1.** Dynamic Light Scattering, Electrokinetic Potential, and Drug Encapsulation Analysis of the Nanoparticle Systems.

| | Quasi Elastic Light Scattering | | Electrokinetic Potential | Drug Encapsulation |
|---|---|---|---|---|
| | Hydrodynamic Diameter (nm) | Polydispersity Index (PI) | Zeta Potential (mV) | Efficiency (%) |
| LNP | 93.6 ± 0.4 | 0.061 | -9.46 ± 0.31 | — |
| HA-LNP | 157.2 ± 1.4 | 0.105 | -38.07 ± 0.35 | — |
| HA-LNP Rehydrated | 182.1 ± 1.2 | 0.201 | -41.24 ± 0.57 | — |
| HA-LNP- 10, 20, or 70 kDa FD | 185 → 200 | 0.15 → 0.21 | -41 → -43 | 35 → 55 |
| HA-LNP - DOX | 175.9 ± 7.5 | 0.233 | -35.24 ± 0.27 | 65.1 ± 4 |

### 2.3.2. **Nanoparticle Stability**

We next investigated the nanoparticle stability in solution over 90 days. As a result of the increased surface charge density of the LNPs following HA surface crosslinking, the interactions between the particles in suspension were now outside the thermodynamic confines of colloidal instability (~|35|mV) [36], yielding a long-term stable nanoparticle suspension. Hyaluronic Acid coated LNPs were validated to be stable and avert bilayer fusion for over three months at 4° Celsius (**Table 2.2**).

**Table 2. 2.** HA coated nanoparticle stability as a function of time. Stability was assessed by changes in particle diameter and surface charge. The HA-LNPs were stored in 4°C during the test.

| | **Quasi Elastic Light Scattering** | | **Electrokinetic Potential** |
|---|---|---|---|
| | Hydrodynamic Diameter (nm) | Polydispersity Index (PI) | Zeta Potential (mV) |
| Day 0 | 164.9 (±) 1.5 | 0.198 | -39.06 (±) 0.43 |
| Day 30 | 168.7 (±) 2.4 | 0.212 | -38.02 (±) 0.97 |
| Day 90 | 170.3 (±) 9.3 | 0.255 | -38.09 (±) 2.43 |

### 2.3.3. **Analysis of Cargo entrapment (20, 70 kDa FD) and DOX**

To test the ability of the HA-LNP nanocarrier system to entrap a range of different therapeutic types, three model drugs were implemented: DOX (0.58 kDa), 20 kDa FITC tagged Dextran (FD), and 70 kDa FD. Following rehydration of the dry lipid powder, an encapsulation efficacy of 65%, 55%, and 35% for the DOX, 20 kDa FD, and 70 kDa FD was achieved respectively **(Table 2.1)**. The decrease in encapsulation efficiency as the therapeutic cargo size increases was expected due to the increased steric force of therapeutic confinement in the aqueous core of the nanoparticle.

### 2.3.4. **TEM**

Transmission electron microscopy was used to characterize the nanocarrier on a per particle basis. TEM characterization of the LNP system exposed that 1) the surface roughness increased post crosslinking to HA, further providing validation of an appreciable coating of the biopolymer on the nanoparticle surface, and 2) that HA is an effective cryoprotectant for LNPs and is required to keep the nano-dimensions of the platform during the drug entrapment process **(Fig 2.4)**.

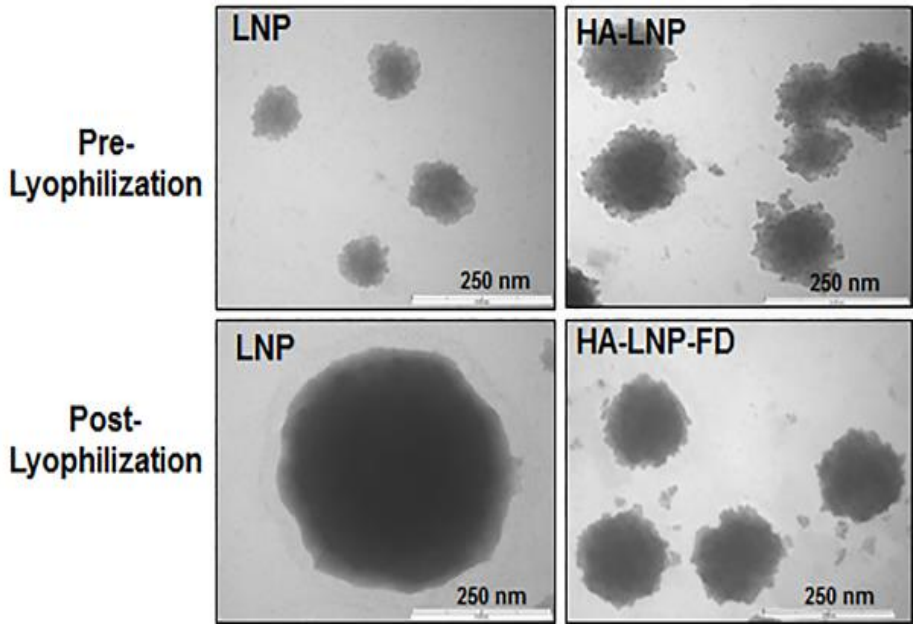


**Figure 2. 4.** Transmission Electron Microscopy (TEM) using the negative stain method with 2% phosphotungstic acid. Scale Bars are 250 nm for TEM.

## 2.4. Conclusions

The commercialization of advanced drug delivery systems has been hindered due to the fabrication of single purpose platforms. While liposomes and lipid based nanoparticles have been used to improve the efficacy of therapeutic drugs, there still

remains a need for the development of a single nanocarrier system that can be used to successfully encapsulate a range of therapeutic types for broad applications with a high potential for scale up. In this study we engineered a lipid nanoparticle system comprised of a core structure of biocompatible lipids and cholesterol, and a surface decorate of high MW HA. We optimized both the HA crosslinking reaction to the nanoparticle surface, as well as the rehydration and entrapment conditions for optimal entrapment efficiency. We modeled a range of therapeutic entrapment by utilizing the fluorescently tagged model drugs: 1) 20 kDa FITC tagged Dextran (20 kDa FD) – model drug for silencing RNA entrapment, 2) 70 kDa FITC tagged Dextran (70 kDa FD) – model drug for protein based therapeutics, and 3) Doxorubicin (DOX) – model drug for small molecule inhibitors and chemotherapeutics.

# CHAPTER 3: INTRACELLULAR DELIVERY OF THERAPEUTICS TO CARDIAC, BRAIN, AND BREAST CELLS VIA THE LIPID NANOPARTICLE SYSTEM

## 3.1. Introduction

The principal objective of a nanoparticle drug delivery system is to capture, protect, and successfully transport a therapeutic cargo to a specific coordinate in the body. During this process, the nanocarrier system must overcome numerous extracellular and intracellular barriers to facilitate the designed function of the therapeutic. In recent years, there has been a significant interest in developing novel drug delivery systems that can successfully promote efficient intracellular delivery of therapeutic cargo, and also evade cellular degradation pathways such as lyosomal entrapment to promote increased drug efficacy [37, 38].

Lipid based nanoparticle (LNP) systems have been successfully employed to mediate intracellular delivery for a variety of therapeutics including protein [39], nucleic acid [40], and small molecule chemotherapeutics [14, 22] amongst others following systemic administration. However, by increasing the circulation time of LNPs via surface coating with polyethylene glycol (PEG) to create stealth particles, studies have seen a marked decrease in cellular uptake efficiency [41]. In addition, since PEG does not favor a specific endocytosis pathway over another, this process cannot be altered to influence the endolysosomal fate of the LNP system. Therefore there is a need to develop a drug delivery platform that mediates efficient intracellular delivery of a range of therapeutics types that can also escape lysosomal degradation and distribute the therapeutic homogenously throughout the cytoplasm.

Herin, we have tested and optimized our previously engineered high MW Hyaluronic Acid (HA) coated LNP system to promote intracellular delivery of therapeutic cargo and evade lysosomal degradation in cardiac, brain, and breast cells *in vitro*. The HA-LNP system promoted uptake of a cell impermeable fluorescent model cargo, FITC-dextran, as compared to the naked form. Furthermore, the HA-LNP system increased the therapeutic index of Doxorubicin by over 30 % compared to the free form of the drug to metastatic breast cancer cells. Confocal microscopy was used to probe the endolysomal fate of HA-LNPs in cardiac, brain, and breast cells leading to validation of cell-dependent cytoplasmic distributions of the nanocarrier system.

## 3.2.Materials and Methods

### 3.2.1. **Cell Culture Protocol**

21MT-1 Cells were a kind gift from Dr. Band at the University of Nebraska Medical Center. This cell line was isolated from the metastatic pleural effusion mammary tumor specimens [42]. The 21MT-1 cells were cultured in α-MEM media supplemented with 5% fetal bovine serum (FBS), 1% Penicillin-Streptomycin (PS), 1% L-glutamine, 20 mM HEPES, non-essential amino acids, sodium pyruvate (all stated reagents from Invitrogen), 12.5 ng/ml epidermal growth factor (EGF) and 1µg/ml hydrocortisone (both from Sigma). SKBR3 (ATCC HTB30), a human HER2+ invasive mammary gland adenocarcinoma cell line, were cultured in analogous conditions as the 21MT-1 cells except without the addition of EGF or hydrocortisone. MCF10A (ATCC CRL-10317), human normal breast tissue cell line, were cultured in DMEM/F12 (Mediatech) and supplemented with 1% L-glutamine, 1 % Penicillin-Streptomycin, 5% Horse Serum, 0.1 ng/ml cholera toxin (Sigma), 0.5 µg/ml hydrocortisone, 10 µg/ml insulin (Sigma), and 0.02 ng/ µl rhEGF (Sigma). HL1 mouse

cardiomyocytes were a kind gift from Dr. Mishra at University of Nebraska-Medical Center (UNMC) and grown in Claycomb Media (Sigma) supplemented with 5 % FBS, 1 % PS, 0.1 mM Norepinephrine (Sigma), and 0.1 mM L-glutamine (Sigma). A172 human glioblastoma cell line (ATCC CRL-1620) were cultured in DMEM (Sigma) media supplemented with 10% FBS and 1 % PS. Primary cerebellum astrocytes were a kind gift from Mrs. Christina Wilson, and cultured in DMEM media supplemented with 10% FBS and 1 % PS. For all cell types, the inclusion of FBS signifies the term "complete media", while the absence of FBS from the media is called "incomplete media". All cells were kept in aseptic conditions, and grown in an incubator at 37°C and 5 % CO2.

### 3.2.2. **Therapeutic Cargo Uptake Experiments**

21MT-1, SKBR3, MCF10A, and HL1 cells were plated in 12 well plates at a seeding density of 100,000 cells/ well and left overnight in complete media to facilitate cell attachment. The next morning the media was switched to incomplete media and 70 pmol of 20 or 70 kDa FD either encapsulated inside HA-LNPs or in the naked form (no nanocarrier) was added to designated wells. After a 5 hour incubation time, the cells were washed three times with 1X PBS followed by visualization with a fluorescent microscope and quantification of FD uptake by a fluorescent plate reader. Both the HA-LNP-FD and naked FD samples were compared to control cells with no FD added to remove specific cell auto-fluorescence.

### 3.2.3. **Flow Cytometry**

Flow cytometry was performed using a FACSCantoII (BD). Two 12 well plates plated with 100,000 A172 or primary cerebellum astrocyte cells/well was cultured overnight within complete media. The media was switched to incomplete media, and select wells

were cultured with 85 μg/well of fluorescently conjugated HA-LNPs (fluorescently tagged cholesterol) for 12 hours. Following the incubation time, cells were washed three times with sterile 1X PBS, trypsinized, transferred to flow cytometry tubes, and analyzed for fluorescence in the green channel (ex. 495, em. 520; 10,000 total events/read) against control cells.

### 3.2.4. **Confocal Microscopy**

Two separate experiments were performed using live cell confocal microscopy: 1) intracellular delivery of 20 kDa FD by HA-LNPs to 21MT-1 cells and 2) analysis of the intracellular fate of the HA-LNPs following endocytosis in 21MT-1, A172, primary astrocytes, and HL1 cardiomyocytes. In both cases, the cells were all plated to 80 % confluency on 35mm glass bottom dishes (Mattek). The first experiment followed analogous procedures described earlier involving cellular incubation with 165 pmol of 20 kDa FD encapsulated inside HA-LNPs for five hours. The second experiment employed the usage of HA-LNPs tagged with 0.15 mass % Top Fluor Cholesterol (Avanti) in the lipid bilayer as a tracker, a five hour incubation of the tagged particles with 21MT-1 cells, and lysosome staining by Lysotracker Red DND 99 (Life Technologies) . In both experiments the cellular nuclei were stained by Hoescht Nuclear Stain 33342 (Pierce). Following the HA-LNP-FD or HA-LNP-tagged incubation and subsequent staining procedure, the cells were washed three times with 1X PBS and visualized with an Inverted confocal microscope (Olympus IX 81) at the UNL Microscopy Core Research Facility.

### 3.2.5. **Potency Assay**

The DOX concentration lethal to 50% of the 21MT-1 cells ($LC_{50}$) was determined utilizing the MTT (3-(4,5-dimethyldiazol-2-yl)2,5 diphenyl Tetrazolium Bromide) assay

kit from Life Technologies (Carlsbad, CA, USA). This classical colorimetric assay assesses cell health as a function of the mitochondrial conversion of MTT salt to Formazan. 21MT-1 cells were seeded at a density of 32,000 cells/well in three 48 well plates with DOX encapsulated inside HA-LNPs. After a 24 hours incubation time, the media was aspirated and 5 mg/ml MTT working solution was added and incubated for 2 hours at 37°C. Cells were then lysed with lysis buffer (acidified IPA) and the absorbance was measured at 570 and 620 nm using a Beckman Coulter AD340 plate reader (Indianapolis, IN, USA). Percent viability was determined by normalization of the 570/620 ratio to the control untreated cells and positive control dead cells.

#### 3.2.6. **Statistical Analysis**

The difference between experimental groups was analyzed by a one-way analysis of variance (ANOVA) in the software package Prism 6 (Graphpad) and by a subsequent Tukey's multiple comparison test. For statistical analysis of all data, $p<0.05$ was taken as the lowest acceptable threshold for significance.

## 3.3.Results and Discussion

#### 3.1.1. **Naked vs HA-LNP encapsulated uptake of FD**

To test the ability of the HA-LNP nanocarrier system to encapsulate and delivery a range of therapeutic cargo, we employed the use of the model drug FITC-Dextran. FITC-Dextran (FD) is a hydrophilic cargo that is 1) cell membrane impermeable, 2) fluorescently tagged, and 3) can be synthesized to a range of molecular weights to model the delivery of different size therapeutics. For cell uptake experiments we specifically chose 20kDa and 70 kDa FD. 20kDa FD is the size of most silencing RNAs for gene delivery applications, where 70 kDa FD is the size of most protein based therapeutics. To address the broad need

for nanoparticle systems as well as to discern the overall efficacy of the HA-LNP platform, we performed cell uptake experiments with heart, breast, and brain cells *in vitro*.

Cardiovascular disease effects an estimated 84 million Americans, causing on average 2,200 deaths per day, and an annual economic cost of over $300 billion dollars in both health expenditures and lost productivity [43]. Novel nanoparticle systems are needed to alleviate this health epidemic via improved delivery of cardiovascular therapeutics. To test our HA-LNP system on cardiac cells, we first incubated HL1 cardiomyocytes with 70 pmol FD (20 kDa or 70 kDa) in either the "naked" (non nanocarrier) form or with an equivalent amount of FD encapsulated inside HA-LNPs (HA-LNP-FD) and compared the uptake qualitatively using a fluorescent microscope and quantitatively using a plate reader (**Fig 3.1**). After a five hour incubation, we observed very low uptake of naked FD and significantly more uptake with the HA-LNP system for both 20 and 70 kDa FD. We also observed higher fluorescent intensity in the HA-LNP- 70 kDa FD sample over the HA-LNP- 20 kDa FD sample due to the higher density of FITC tagging on the longer chain dextran. Overall this experiment validated the successful encapsulation and uptake of a cell impermeable cargo mediated by the HA-LNP system to cardiovascular cells.

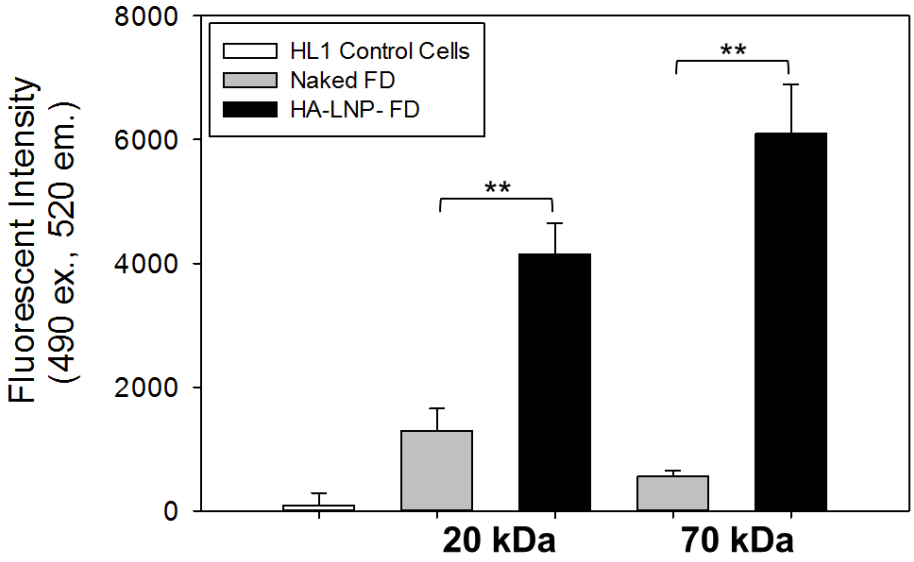


**Figure 3. 1.** Analysis of the cardiomyocyte (HL1) uptake of 20 and 70 kDa FD model drug in vitro. The model drug was utilized in two distinct forms: 1) encapsulated inside the aqueous core of HA-LNPs and 2) naked (no association with a nanocarrier). Plate reader quantification five hours post addition of the naked FD or HA-LNP-FD (*P<0.05, **P<0.005, ***P<0.0001; n=3).

We next performed the analogous FD uptake procedure on breast cell lines *in vitro*. Breast cancer is the second leading cause of death for women in the United States with current projections for 2015 forecasting over 230,000 newly diagnosed invasive cases and 40,000 resultant deaths [44]. Consequently, it is extremely important to be able to successfully delivery a range of therapeutic drugs into breast cells. Three developmentally distinct human breast cell lines were chosen for nanoparticle uptake analysis: 1) MCF10A (normal mammary epithelial cells), 2) SKBR3 (HER2+ invasive breast cancer cells), and 3) 21MT-1 (stable patient-derived metastatic breast cancer cells isolated from the metastatic pleural effusion) **(Fig 3.2)**. We observed that the fluorescence intensity was significantly higher in all three cell types when FD was delivered using HA-LNPs as

compared to naked delivery. Furthermore, the metastatic cell line had the highest fluorescence intensity compared to other cell lines indicating that the uptake of the LNPs was highest in the metastatic cells. This experiment signified that there was a strong correlation between uptake of the HA-LNP-FD particles and the degree of the breast tissue malignancy.

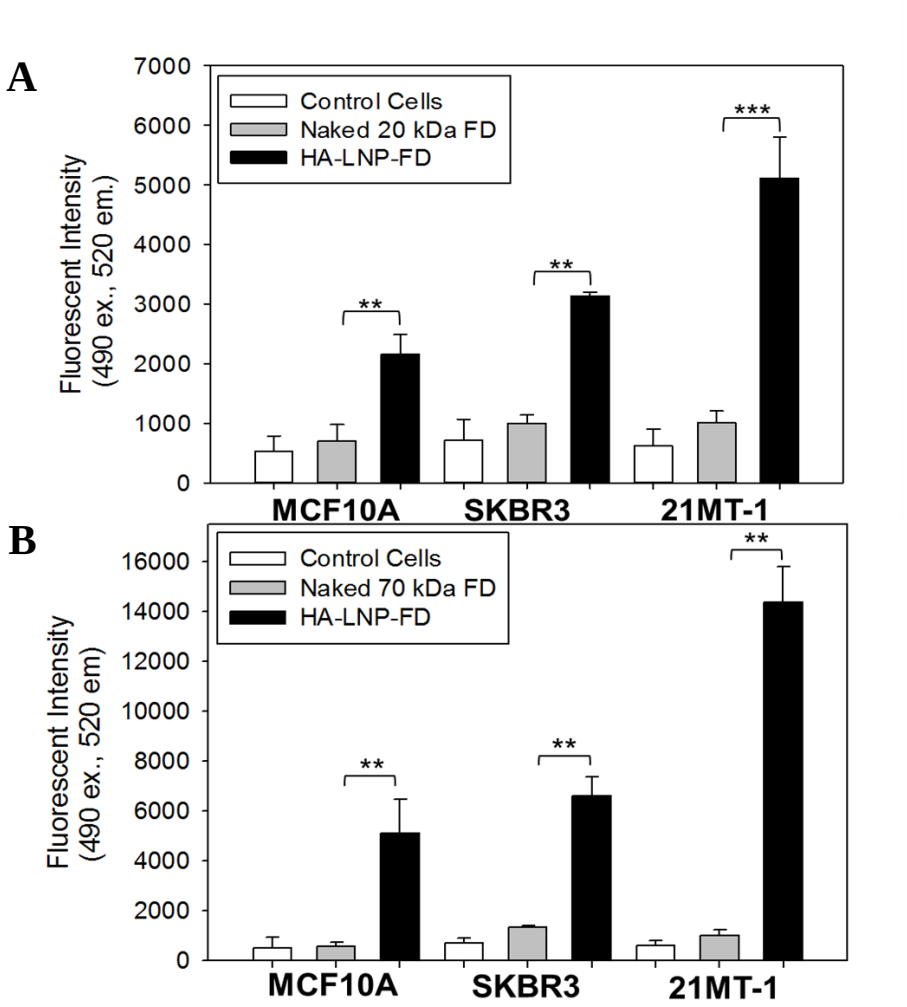


**Figure 3. 2.** Analysis of the cellular uptake of FD model drug to human breast cell lines in vitro. The model drug was utilized in two distinct forms: 1) encapsulated inside the aqueous core of HA-LNPs and 2) naked (no association with a nanocarrier). Plate reader quantification five hours post addition of the naked FD or HA-LNP-FD. (A) 20 kDa; (B) 70 kDa (*P<0.05, **P<0.005, ***P<0.0001; n=3).

To validate the fluorescent intensity via the HA-LNP system was intracellular and not due to FD residing on the outer cell membrane as a result of the adhesive nature of liposomes, we also performed live confocal microscopy with the 21MT-1 cell line following incubation with HA-LNP-20kDa FD **(Fig 3.3)** and HA-LNP-70 kDa **(Fig 3.4)**. This experiment clearly demonstrated the intracellular delivery of both 20 kDa and 70 kDa FD with the HA-LNP system.

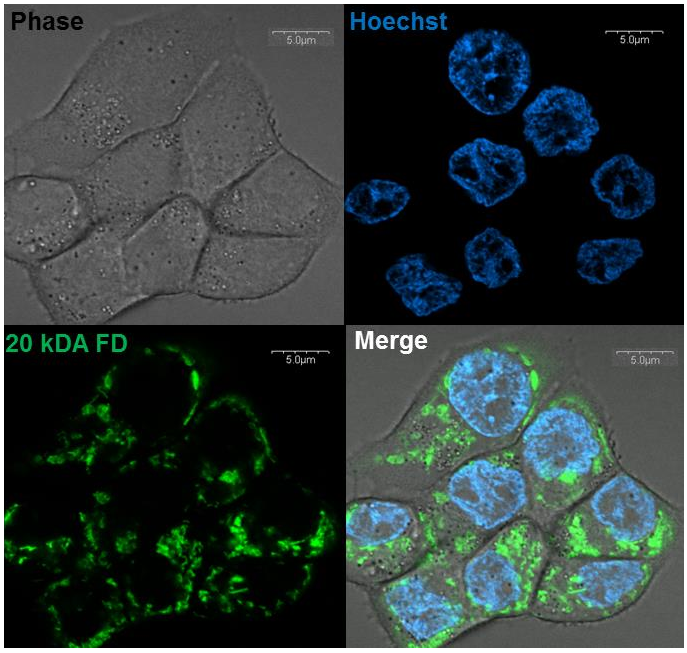


**Figure 3. 3.** Live confocal microscopy was used to validate the intracellular delivery of the 20kDa FD cargo from the HA-LNP-FD nanocarrier: A cluster of 21MT-1 breast cancer cells at 100x magnification with optical zoom (Scale bars are 5µm).

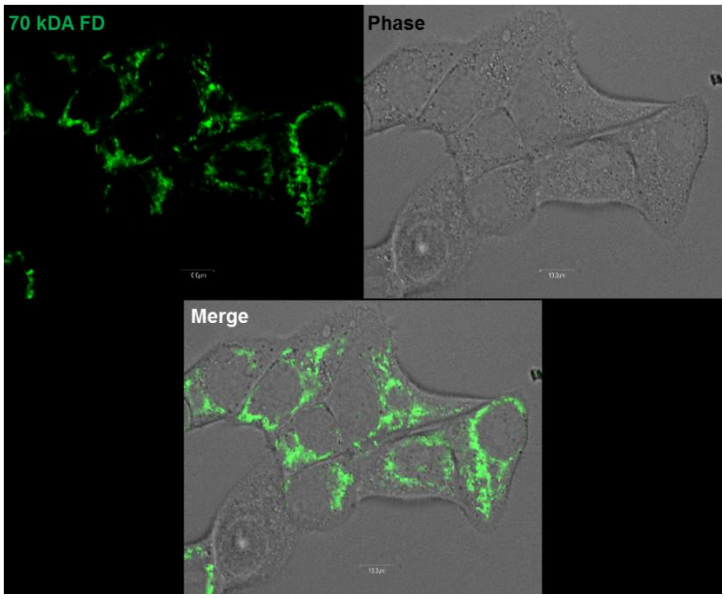


**Figure 3. 4.** Live confocal microscopy was used to validate the intracellular delivery of the 70kDa FD cargo from the HA-LNP-FD nanocarrier: A cluster of 21MT-1 breast cancer cells at 100x magnification with optical zoom (Scale bars are 10µm).

The last disease model we addressed in this study is Glioblastoma. Glioblastoma is an aggressive brain tumor arising from astrocytes that occurs in 12 to 15 percent of all intracranial tumors and has a mean survival of 14.6 months [45]. Recently, liposomes and lipid based nanocarrier systems have gained attention as a promising tool for drug delivery through the blood brain barrier [12, 46]. However, there still remains a need for further development in this area to achieve a platform capable of long term glioblastoma disease management. To test our HA-LNP platform for therapeutic delivery to the brain, we used flow cytometry to compare the per cell uptake of our HA-LNPs. In this experiment we tagged our HA-LNPs with 0.15 mass % fluorescent conjugated cholesterol and incubated an analogous concentration of nanoparticles to two different brain cell types: 1) rat primary cerebellum astrocytes and 2) A172- a human glioblastoma cell line. Five hours after nanoparticle addition, we quantified the fluorescent uptake in a

per cell basis and observed a preferential uptake of particles to the glioblastoma cells over the primary cerebellum astrocytes **(Fig 3.5)**. In addition to metabolic effects altering the cellular endocytosis rate, we are currently investigating the difference in surface receptors between the brain cells to determine the difference in cellular uptake.

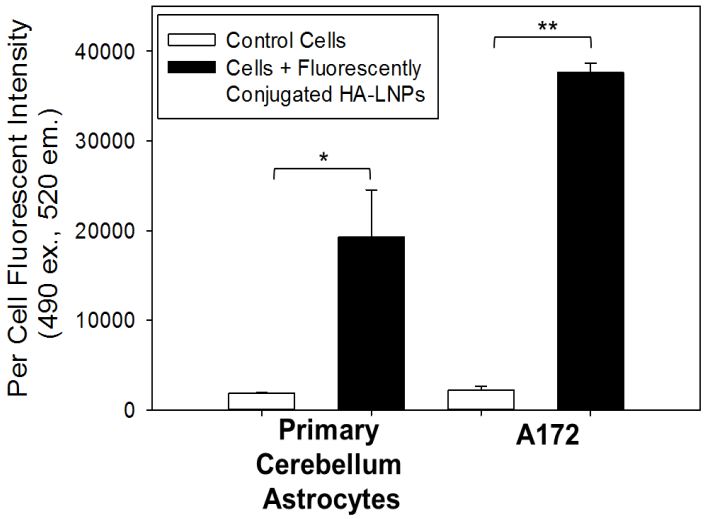


**Figure 3. 5** Analysis of the cellular uptake of fluorescently conjugated HA-LNPs to primary rat cerebellum astrocytes and a human glioblastoma cell line (A172). The fluorescent HA-LNPs were added, and analyzed for per cell fluorescent intensity via flow cytometry five hours post addition (*P<0.05, **P<0.005, ***P<0.0001; n=3).

### 3.1.2. **Potency Assay with DOX**

Following validation that the HA-LNP carrier can be used for model therapeutic delivery into cardiac, breast, and brain cells in vitro, we next wanted to determine the efficacy of the HA-LNP to deliver a bioactive drug to probe the true therapeutic benefit of the HA-LNP system. Doxorubicin (DOX) is a commonly employed chemotherapeutic anticancer drug with natural fluorescent properties. To determine the efficacy of delivering encapsulated chemotherapeutics within the LNP nanocarrier, we performed a potency

assay between free DOX and HA-LNP-DOX with the 21MT-1 metastatic breast cancer cell line **(Fig 3.6)**.

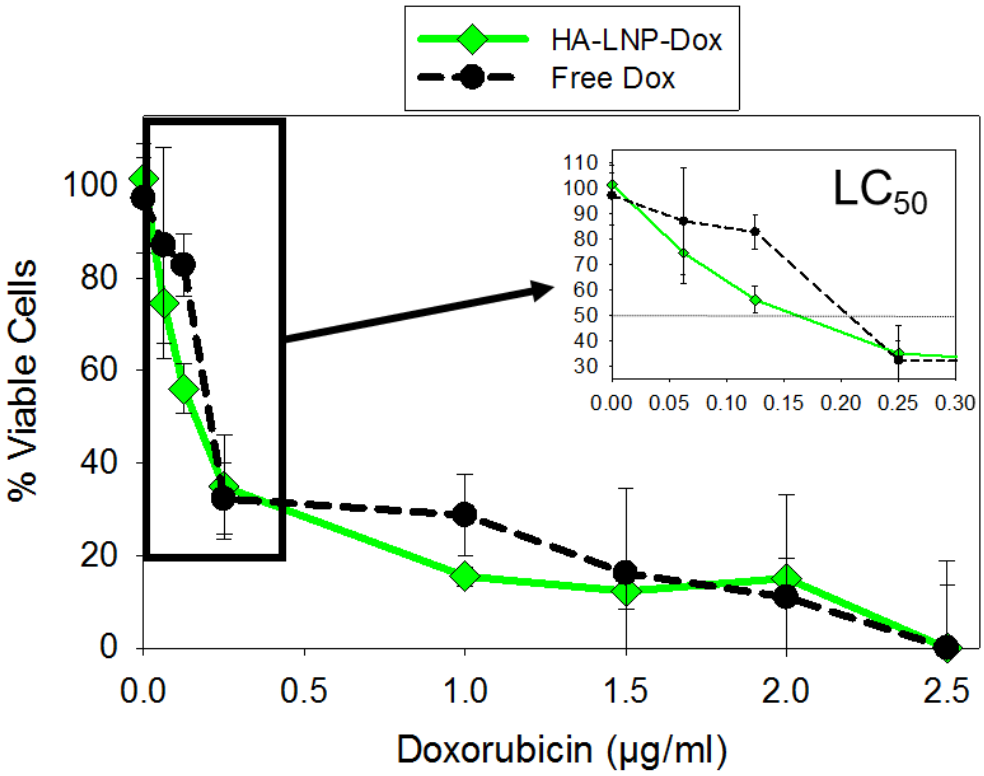


**Figure 3. 6.** Doxorubicin potency assay comparison between Free Dox and DOX encapsulated in HALNPs (HA-LNP-DOX). Standard MTT protocol was used to determine the % viable cells at 24 hours.

The potency assay exposed that the lowest lethal concentration to kill 50% of the cells ($LC_{50}$) was 0.191±0.030 µg/ml and 0.136±0.025 µg/ml for free DOX and HA-LNP-DOX respectively (**Table 3.1**). This data shows that a 30% increase in therapeutic index of DOX was achieve via intracellular delivery in HA-LNPs. As a control, a potency assay with empty HA-LNPs (no DOX) was performed. We observed no toxicity at lipid levels 100

times higher than the concentrations used in the DOX potency assay, thus demonstrating that the lipid nanocarrier is an efficient and non-toxic delivery system **(Fig 3.7)**.

**Table 3. 1.** Potency assay summary ($LC_{50}$ values) between the free form DOX, and HA-LNP encapsulated DOX to 21MT-1 Metastatic Breast Cancer Cells at 24 hrs.

| Delivery Method | $LC_{50}$ (µg/ml) |
|---|---|
| Free Dox | 0.191 ± 0.0301 |
| HA-LNP-DOX | 0.136 ± 0.0248 |

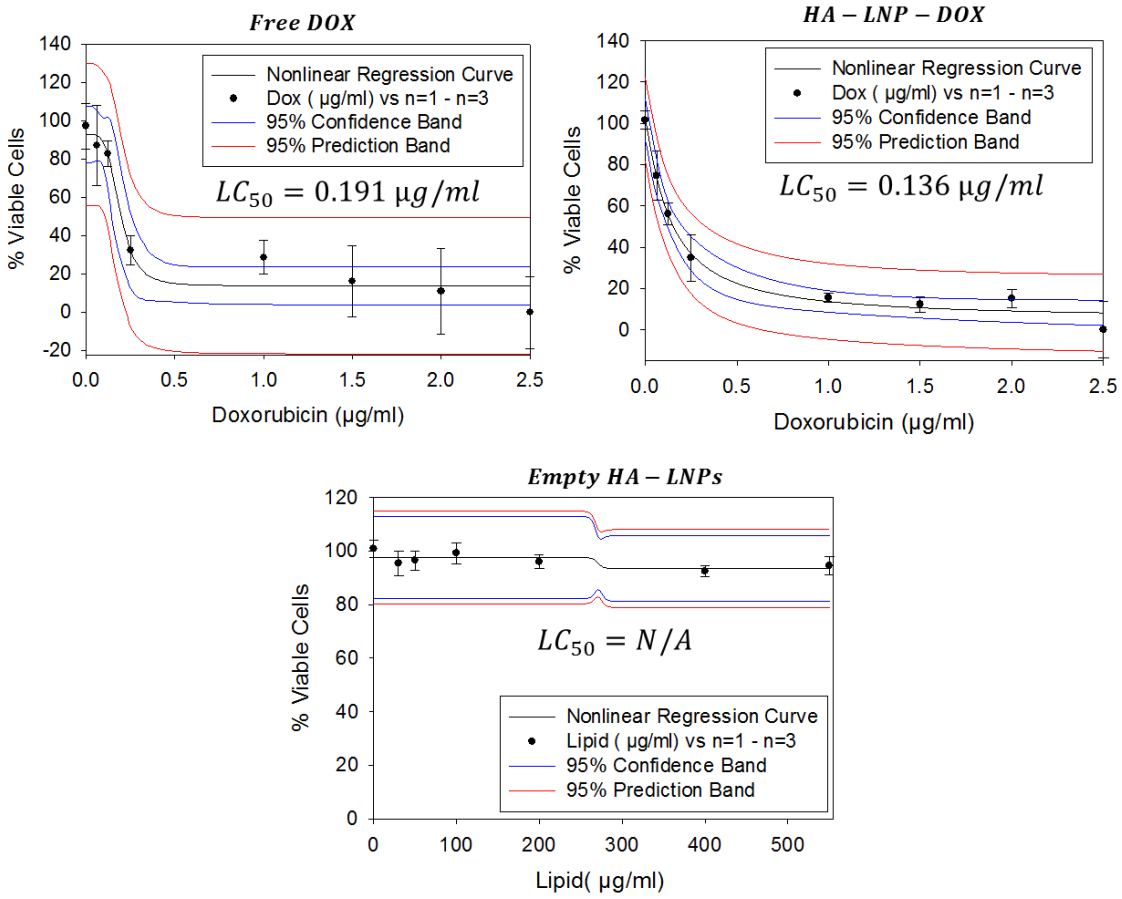


**Figure 3. 7.** $LC_{50}$ nonlinear regression curves with both confidence and prediction bands for the 24 hr. potency assay comparison between the HA-LNP- DOX and free form DOX in 21MT-1 metastatic breast cancer cells.

### 3.1.3. **Endolysosomal Tracking of Fluorescently Tagged HA-LNPs**

For the successful implementation of the HA-LNP system for drug delivery applications, the nanocarrier itself must evade lysosomal degradation so the therapeutic cargo can escape to the cytosol to perform its intended function. To probe the endolysosomal fate of the HA-LNP system, we utilized our green fluorescent cholesterol tagged HA-LNPs and performed live confocal microscopy. We first plated 21MT-1 cells, incubated the cells with tagged HA-LNPs, stained cellular lysosomes (a main degradation pathway for nanoparticles) red, and found minimal co-localization between the lysosomes and our HA-LNPs **(Fig 3.8A)**. In addition, we found that our HA-LNPs were homogenously dispersed in the cellular cytoplasm, signifying endosomal escape. In order to validate that the HA-LNPs were cytosolic, we performed a z-axis transformation to construct a side profile view of the cells (XZ plane view: the bottom of the XZ plane is the contact point between the cells and the petri dish) **(Fig 3.8B)**. We used the nucleus as an internal reference point in this construct to validate the nanoparticles were in fact cytosolic and not residing on the outer cellular membrane. In this z-axis transformation analysis the HA-LNPs also appeared uniform in dispersion with virtually no co-localization with lysosomes.

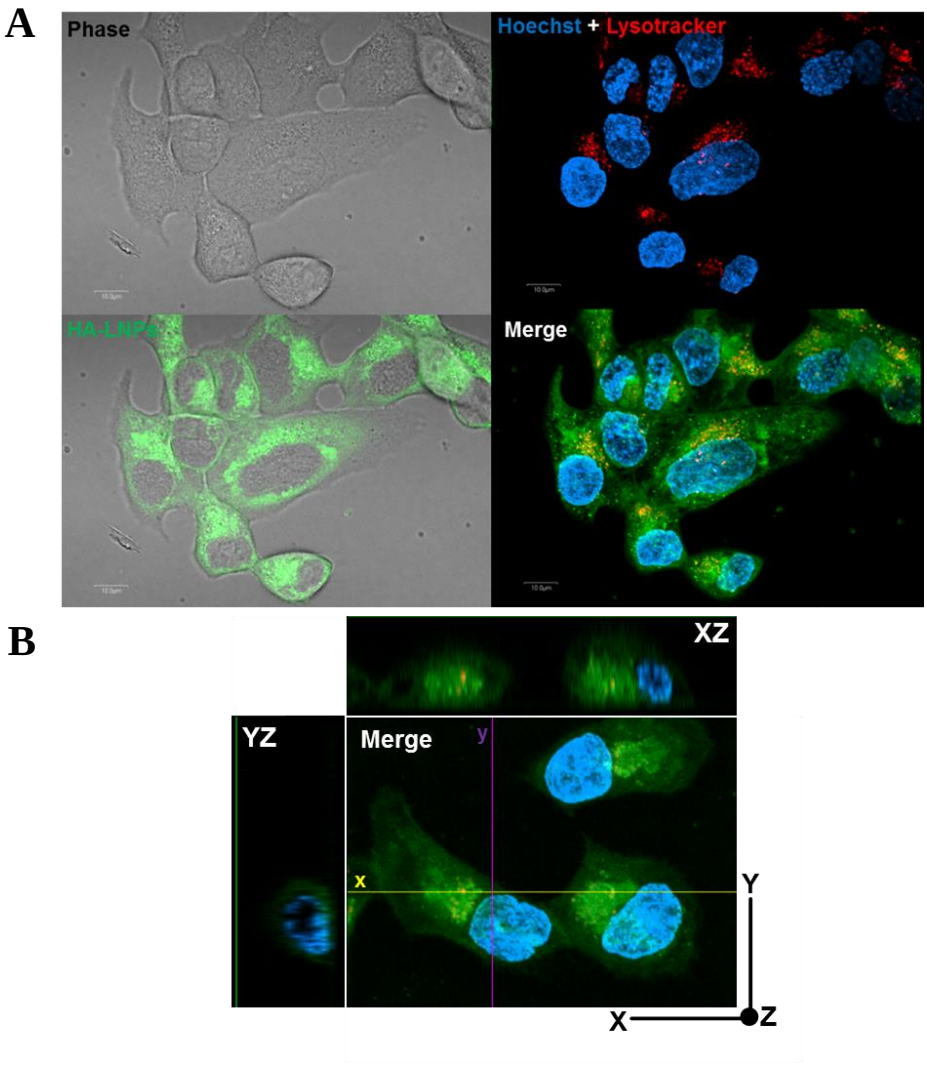


**Figure 3. 8.** Live confocal microscopy analysis of HA-LNP localization in the 21MT-1 metastatic breast cancer cell line in vitro. HA-LNPs with 0.15 mass % FITC tagged cholesterol in the lipid bilayer of the nanoparticles was used to track nanoparticle - endocytosis into the cell. (A) The cholesterol tagged HA-LNPs were incubated with the 21MT-1 cells for 5 hours and measured for co-localization with lysosomes to determine the fraction of viable therapeutic that escapes the nanoparticle degradation pathway. (B) Confocal Microscopy with a Z-axis transformation of 21MT-1 cells at 100x zoom was used to validate cytoplasmic delivery by using the nucleus as a reference point inside the cell (The XZ plan shows the height and width of the cell).

We also performed the tagged HA-LNP incubation and confocal microscopy analysis with cardiomyocytes cells to probe cell-dependent endolysosomal fate (**Fig. 3.9**). A much higher amount of co-localization occurred between the HA-LNPs and the lysosomes in the cardiac cells, signifying more lysosomal entrapment and subsequent HA-LNP degradation. This may be due to the increased lyosomal activity of this cell type over the metastatic breast cancer cell line, or the change in the endocytosis pathway used by the HA-LNPs.

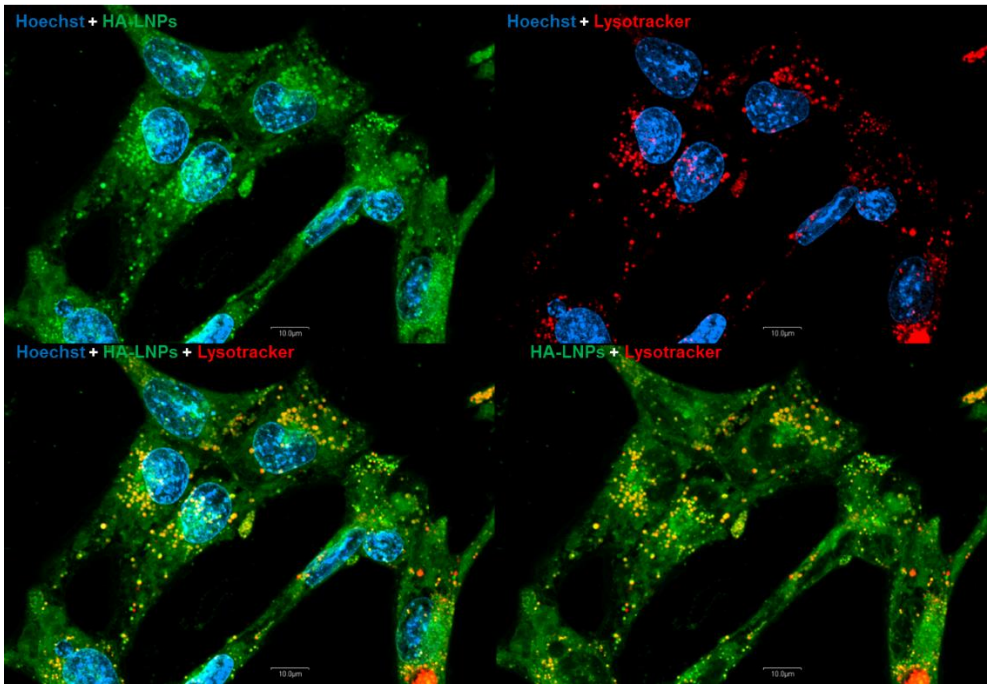


**Figure 3. 9.** Live confocal microscopy analysis of HA-LNP localization in the HL-1 mouse cardiomyocyte cell line *in vitro*. HA-LNPs with 0.15 mass % FITC tagged cholesterol in the lipid bilayer of the nanoparticles was used to track nanoparticle - endocytosis into the cell. The cholesterol tagged HA-LNPs were incubated with the HL-1 cells for 5 hours and measured for co-localization with lysosomes to determine the fraction of viable therapeutic that escapes the nanoparticle degradation pathway.

Lastly, we compared the endolysosomal fate of primary cerebellum astrocytes and glioblastoma cells **(Fig 3.10)**. This experiment exposed a very high uptake of HA-LNPs into the glioblastoma cells, with minimal co-localization with lysosomes albeit high

lysosomal activity present in the cell **(Fig 3.10 A)**. However the uptake of HA-LNPs in primary cerebellum astrocytes was significantly lower, and expressed higher lysosomal entrapment. These HA-LNP uptake results match the flow cytometry output achieved earlier.

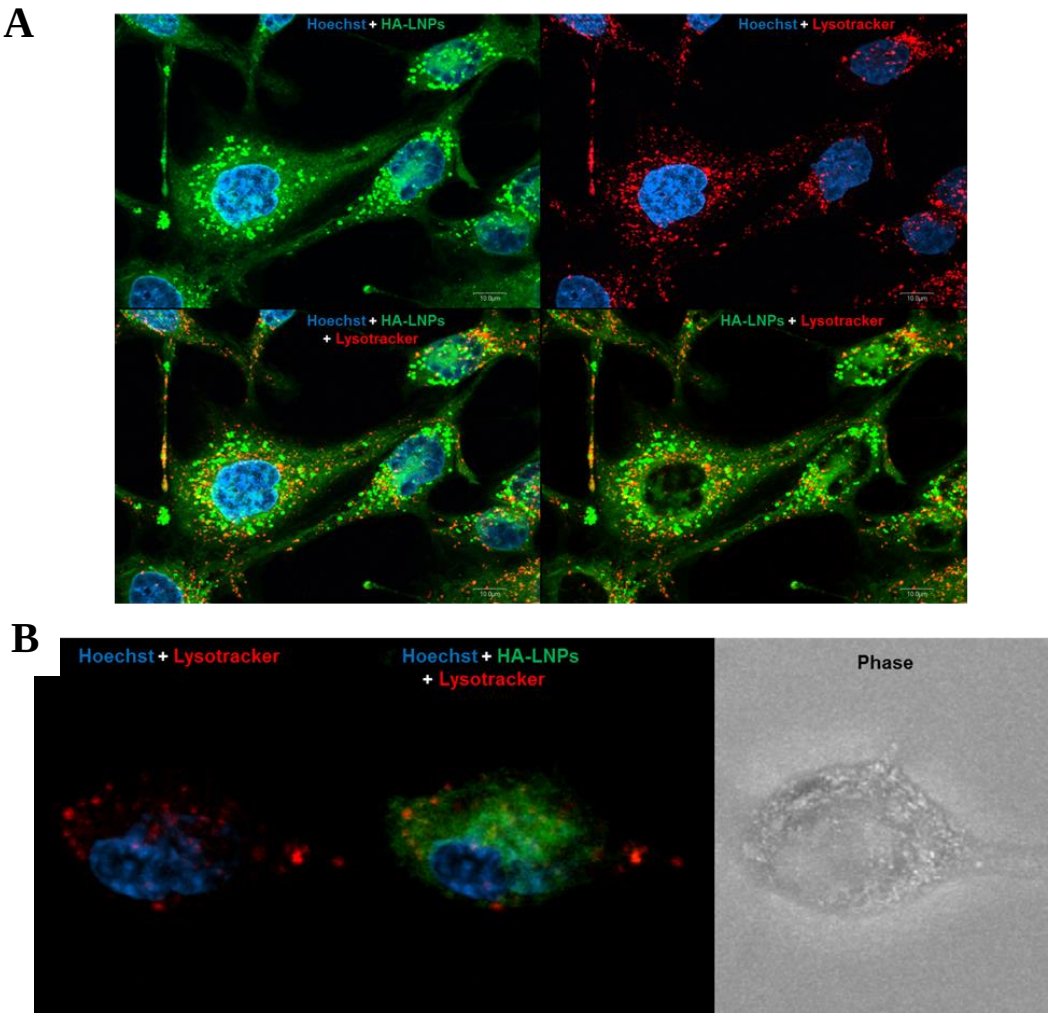


**Figure 3. 10.** Live confocal microscopy analysis of HA-LNP localization in brain cells *in vitro*. HA-LNPs with 0.15 mass % FITC tagged cholesterol in the lipid bilayer of the nanoparticles was used to track nanoparticle - endocytosis into the cell. The cholesterol tagged HA-LNPs were incubated with the (A) A172 human glioblastoma cell line or (B) Primary rat cerebellum astrocytes for 5 hours and measured for co-localization with lysosomes to determine the fraction of viable therapeutic that escapes the nanoparticle degradation pathway.

## 3.4. Conclusions

The efficacy and ultimate employment of a nanocarrier system for disease management is dependent upon the successful intracellular delivery of a therapeutic cargo. In this study, the HA-LNP system was shown to facilitate uptake of a cell impermeable fluorescent model cargo, FITC-dextran. Furthermore, the HA-LNP system increased the therapeutic index of Doxorubicin by over 30 % compared to the free form of the drug to metastatic breast cancer cells. Lastly, confocal microscopy was used to probe the endolysomal fate of HA-LNPs in cardiac, brain, and breast cells leading to validation of cell-dependent cytoplasmic distributions of the nanocarrier system.

# CHAPTER 4: EFFECT OF SUBSTRATE STIFFNESS ON LIPID NANOPARTICLE UPTAKE

## 4.1. Introduction

The mechanics of the cellular microenvironment such as physical cues from the extracellular matrix (ECM) greatly influence cellular processes such as proliferation, migration, and differentiation [47]. Furthermore, the transition of epithelial cells from healthy to a malignant phenotype has been shown to be accompanied with structural changes in the local ECM leading to increased stiffness [48] , hindered diffusion [49, 50], and deregulated ECM expression and dynamics [51, 52]. As a result of this transition, the efficacy of chemotherapeutics for the treatment of cancerous tumors has been shown to be reduced [53]. To date, multiple nanocarrier systems and novel methods have been developed to not only circumvent, but to harness the diffusional constraints of tumor sites for targeting purposes [54]. However, the direct relationship between the local ECM stiffness effect on cells and nanoparticle uptake has not been thoroughly investigated.

Tumor tissues have been observed to exhibit stage specific stiffness profiles during malignancy progression [48]. If the ECM plays a central role in cellular processing, it would make sense that changes in ECM stiffness effects nanoparticle uptake. Although numerous studies have been performed analyzing specific attributes of nanoparticles that effect uptake efficiency, there is a need to better understand how changes in the mechanics of the cellular microenvironment effects nanoparticle uptake.

Herein we utilized a highly tunable dual polymer system to create an array of 2D gel substrates with stiffness ranging from 2 kPa to 70 kPa. We employed the 21MT-1 metastatic breast cancer cell line due to its ability to mimic *in vivo* cancer development

and behavior within the *in vitro* enviroment in a stage dependent manner. We utilized our previously engineered and optimized hyaluronic acid coated lipid nanoparticles (HA-LNPs) to validate that both the stiffness range chosen was able to significantly alter the phenotype of the 21MT-1 cells and that the HA-LNPs were able to achieve homogenous cytoplasmic distribution in cells cultured on varying stiffness. Furthermore, we directly probed nanoparitcle uptake as a function of susbtrate stiffness at multiple times points via per cell and population wide flow cytometry analysis.

## 4.2.Materials and Methods

### 4.2.1. **PDMS Gel fabrication**

To create the polymer substrates of varying stiffness, Sylgard 527 and Sylgard 184 (both from Dow Corning) were mixed in specific mass ratios following a previously reported procedure [55]. The 184:527 mixtures were combined, thoroughly mixed to a single consistent solution, and added to designated tissue culture dishes. The polymer gels were then cured overnight at 65℃ to facilitate crosslinking. For cell culture experiments, the gels were activated in an oxygen plasma cleaner to induce a net negative surface charge, and surface coated with fibronectin (Sigma) to promote cell adhesion. The polymer containing plates were then UV sterilized for over twelve hours in a biosafety cabinet.

### 4.2.2. **Gel Stiffness Characterization**

In order to measure the stiffness of PDMS substrates, the PDMS precursors Sylgard 527 and Sylgard 184 were directly mixed in the required weight ratio in the multiwell culture plates followed by overnight crosslinking. Measurement of Young's Modulus was carried out using TMS-Pro texture analyzer (Food Technology Corporation, Sterling,

VA). The height and diameter of the PDMS discs were measured using a caliper. The samples were compressed 0.2mm and the force and corresponding displacement were recorded and used to construct stress-strain curves. Young's Modulus values were determined from the linear regions of the stress-strain curve.

## 4.3.Results and Discussion

### 4.3.1. **Polymer Substrate Characterization**

To probe the effect of substrate stiffness on lipid nanoparticle (LNP) uptake, we first fabricated and characterized our polymer gel substrates. The substrates were made from a specific ratio of sylgard 184 and sylgard 527 polymers following a previously established protocol [55]. The substrates were cured overnight at 65 °C, allowed to cool to room temperature, and characterized by young's modulus measurements (**Fig.4.1**). We specifically created four different polymer substrates with stiffness ranging from 2 kPa (healthy tissue) to 70 kPa (stiffer than high grade invasive ductal carcinoma) [56] to model the stage dependent cancer progression effects on the tumor microenvironment for breast tissue.

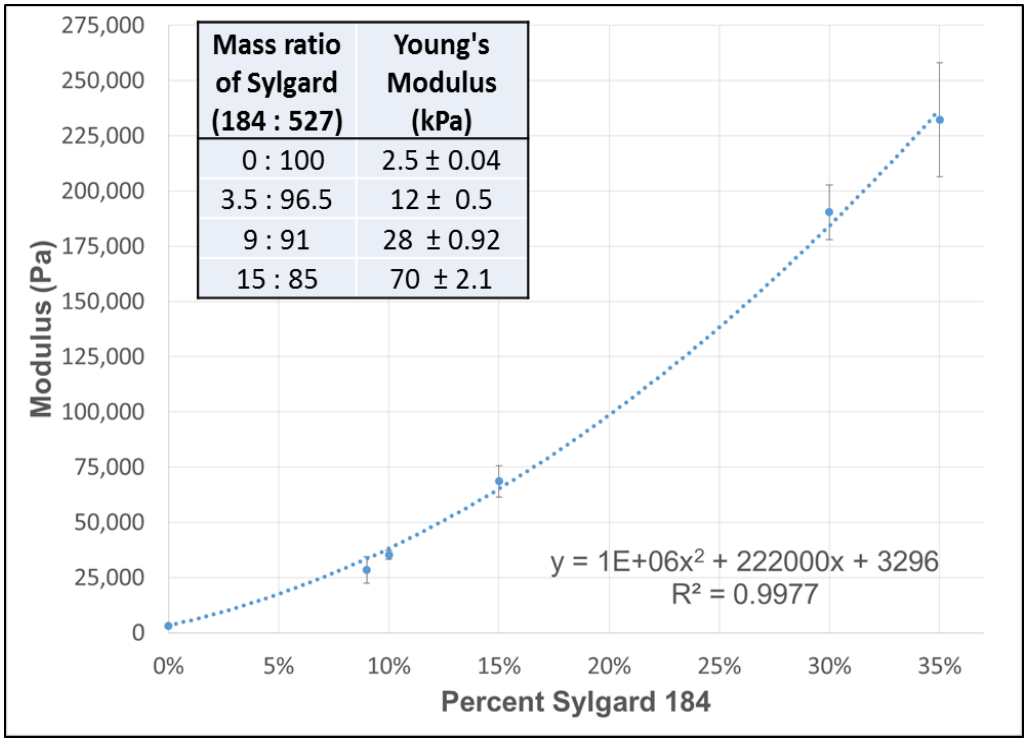


**Figure 4. 1.** Young's Modulus as a function of percent sylgard 184 polymer. This figure shows the tunability of the sylgard polymers to create and range of specific stiffness 2D gel substrates. The inserted table is the stiffness measurements for the four specific polymer substrates chosen: 2kPa, 12 kPa, 28 kPa, and 70 kPa (n=3).

### 4.3.2. **Cell Morphology changes as a function of substrate stiffness**

Following characterization, the polymer substrates were plasma treated to activate the surface, coated with fibronectin to facilitate cell adhesion, and UV sterilized overnight. The next day, 21MT-1 cells were seeded on the substrates and allowed to attach and grow for 24 hours. We specifically chose 21MT-1 cells due to recent reports highlighting the 21T cell line's ability to mimic *in vivo* cancer development and behavior within the *in vitro* enviroment through stage specific cell proliferation, migration, morpholgy, polarization, and gene expression profiles, and its consequent potential for usage as a valuable translational disease model for breast cancer [57].

In order to assess changes in morphology of the 21MT-1 cells following attatchment to the different stiffnes substrates, we employed our previously optimized fluorescently tagged HA-LNP nanocarrier system followed by confocal microscopy analysis (**Fig 4.2**). We have previously shown the efficent uptake and homgenous cytoplasmic distribution of HA-LNPs into 21MT-1 cells on standard tissue culture petri dishes. Therefore, we utilized our fluorescently tagged HA-LNPs to highlight the difference in cell morphology on the different stiffness substrates.

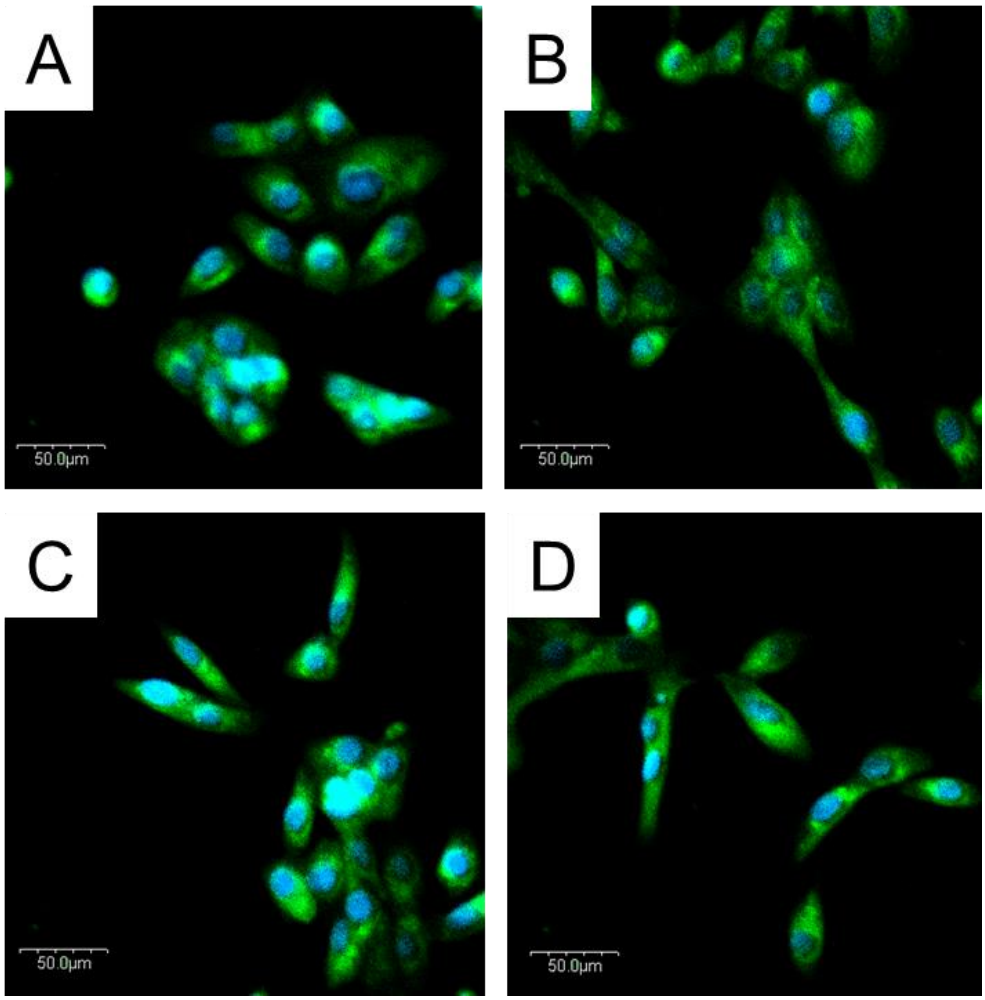


**Figure 4. 2.** 21MT-1 metastatic breast cancer cells morphology depends on substrate stiffness. Confocal microscopy of fixed 21MT-1 cells atop (A) 2kpA, (B) 12.5 kPa, (C) 28 kPa, and (D) 70 kPa for 24 hours, followed by incubation with fluorescently tagged

HA-LNPs (green signal) for six hours. The blue is from the Hoescht nuclear stain. The scale bar is 50μm.

Confocal microscopy analysis of the 21MT-1 cells six hours after HA-LNP addition revealed a drastic change in cellular morphology between the soft to stiff substrates. On the soft 2 kPa substrate, the cells exhibited a spherical morphology indicative of a low stress environment. However, as the substrate stiffness increased, the cell elongation also increased. This phenomena has been seen in various other cell systems on varying stiffness substrates [47, 55, 58]. This experiment validated the phenotypical changes of the 21MT-1 cells as a function of stiffness, as well as the cytoplasmic delivery of the HA-LNPs on the different 2D gel substrates.

### 4.3.3. **Nanoparticle uptake as a function of stiffness**

To directly probe the effect of substrate stiffness on LNP uptake, we incubated a constant amount of fluorescently tagged HA-LNPs with 21MT-1 cells on each of the 2, 12.5, 28, and 70 kPa stiff polymer substrates. Flow cytometry was then performed to discern the stiffness effect on nanoparticle intracellular uptake at both 6 and 12 hours post addition of the HA-LNPs **(Fig 4.3)**.

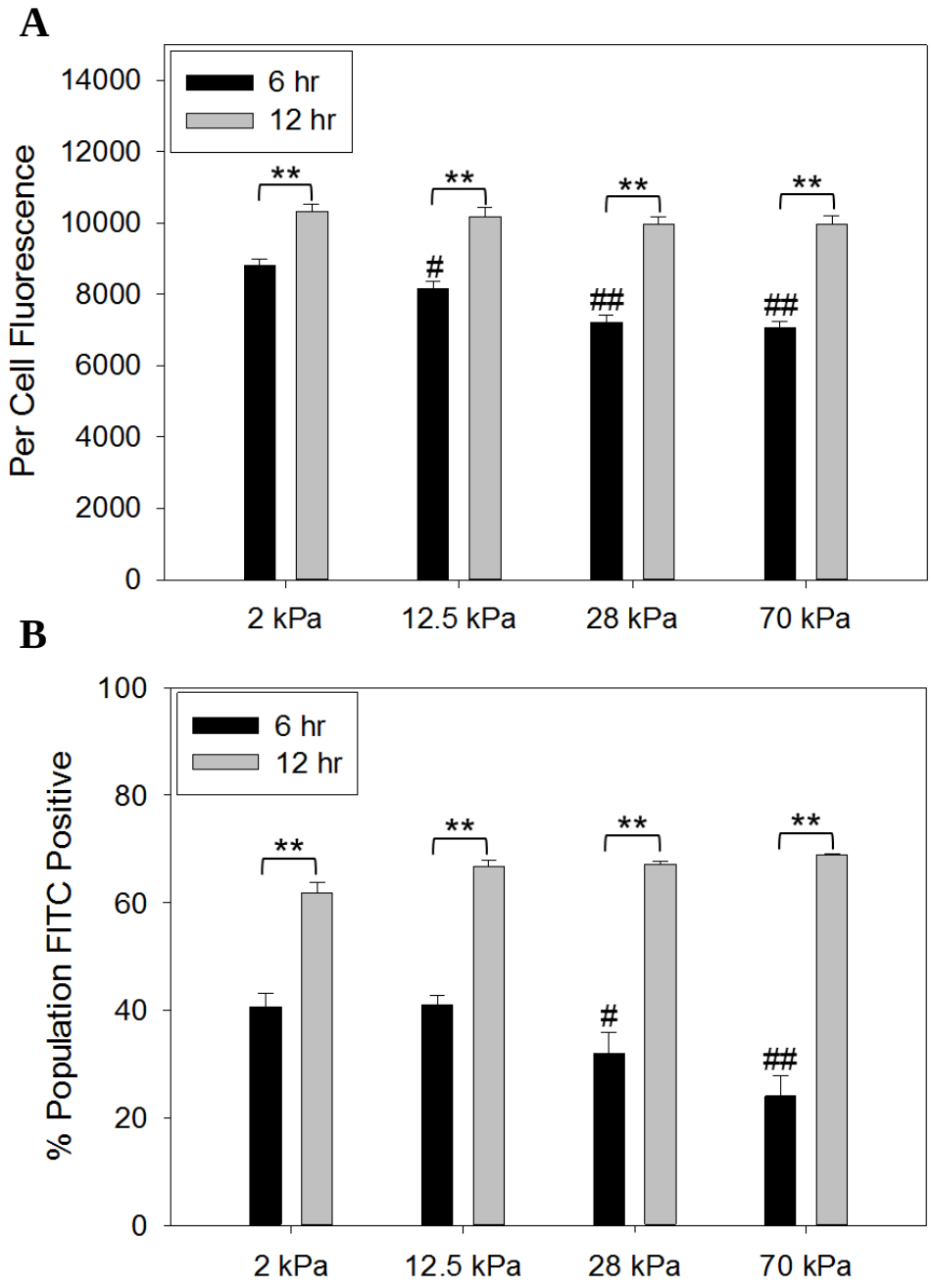


**Figure 4. 3.** Flow Cytometry analysis of fluorescently conjugated HA-LNP uptake as a function of substrate stiffness: (A) Per cell fluorescent analysis and (B) % percent population FITC positive (*P<0.05, **P<0.005, ***P<0.0001; n=3, # denotes significance between the 2kPa and the sample marked following the same significance level designations as the stars).

Interestingly, at the six hour time point an inverse correlation between substrate stiffness and amount of nanoparticle uptake (per cell fluorescence) was observed. The soft substrate exhibited significantly higher HA-LNP as compared to the other stiffer substrate systems. We hypothesize that may be a result of either the reduction in the cell membrane tension of the cells on the soft substrate mediating the higher amount of internalized HA-LNPs [59], or a change in the endocytosis route of the HA-LNPs on different stiffness substrates. However, this preferential uptake mechanisms appears to be quenched at later time points. At the twelve hour time point, all four of the different substrate systems exhibited the same degree of HA-LNP uptake per cell.

A similar outcome was also observed for the analysis of the percent 21MT-1 population FITC positive (i.e. the percent population that has internalized the HA-LNP particles) **(Fig 4.3 B)**. At the six hour time point, cells on the 2 kPa and 12.5 kPa substrates exhibited significantly broader HA-LNP uptake as compare to the stiffer 28 and 70 kPa. However, at the twelve hour time point, the percent population FITC positive was actually highest for the stiffest substrate.

The results from this stiffness-nanoparticle uptake experiment are very important in designing next generation drug delivery systems. The data clearly demonstrates a transient preferential mechanism in which 21MT-1 cells on soft substrates have an initial accelerated nanoparticle uptake both per cell and across the entire cell population, but the overall capacity for HA-LNP uptake between all the substrates is equivalent and matched at the twelve hour time point. This initial enhanced uptake to cells on soft substrates should be further examined to determine if the mechanism is cell dependent or cell

independent phenomena. This information can ultimately be used to develop novel drug delivery systems capable of increased specificity and rate of intracellular delivery.

## 4.4. Conclusions

The ECM undergoes dramatic structural and mechanical changes during tumor progression resulting in altered local stiffness and diffusion patterns. While these changes in diffusion have been thoroughly investigated and taken into consideration in the development of drug delivery systems, the effect of stiffness on nanoparticle uptake in cells is not currently clear. In this study, we used a polymer system to create four physiologically relevant 2D substrates with stiffness ranging from 2kPa to 70 kPa. We first delivered our fluorescently conjugated HA-LNPs to 21MT-1 cells cultured on the polymer substrates of varying stiffness and performed confocal microscopy to validate 1) homogenous cytoplasmic distribution of the HA-LNPs and 2) the morphology of the cells was affected by substrate stiffness indicating phenotypical changes. We then probed the direct effect of substrate stiffness on nanoparticle uptake, and found an initial preferential uptake of HA-LNPs to cells on soft substrates both per cell and population wide. However, at later time points we found that the overall capacity for HA-LNP uptake between all the substrates is equivalent, signifying the effect of HA-LNP is transient. Further analysis of this mechanism could lead to the development of future drug delivery platforms with increased intracellular delivery efficiency and specificity.

# CHAPTER 5: FUTURE WORKS

## 5.1. Targeted Nonviral Gene Delivery *in vitro* and *in vivo*

Recently, liposomes and lipid-based nanoparticles have gained attention as a promising tool for advanced drug delivery to various coordinates of the body including hard to access regions such as the brain [12, 46]. Liposomes, also referred to as vesicles, are extremely versatile carriers that have been studied and utilized extensively for drug delivery applications due to their ease of creation, large protective hydrophilic inner cavity for encapsulation, high degree of freedom for exterior customization, and controllable drug release kinetics. Several preclinical studies using drug-encapsulated liposomes have shown improvement in the sustained release of the cargo, prolonging of the drug's half-life and increasing the therapeutic index of corresponding drug [60]. In addition, numerous drug formulations built on a lipid based platform are currently on the market including Ambisome [17], Doxil [11] and Epaxal [18] with many more in clinical development [61, 62]. These examples of proven success alleviate any questions regarding the clinical viability of liposomal or lipid based platforms as a translational delivery vehicle for gene delivery. The combination of developing targeted delivery mechanisms with the labeling of important biomarkers has advanced *in vivo* application of lipid based carriers by optimizing drug dosage and reducing off-target effects/resultant toxicity. For example, antibody surface modified liposomes were used for targeted siRNA delivery and they successfully silenced genes in leukocytes and reversed experimentally induced colitis in mice while their naked counterparts (not encapsulated in liposome) provided no therapeutic value [63]. While previous research has been performed in the field of silencing RNA gene regulation and its use as an intervention

tool in disease diagnosis and prevention, there have been minimal proposed lipid based delivery platforms for gene delivery.

## 5.2.Substrate Mediated Drug and Gene Delivery System

The engineering of drug delivery platforms facilitating spatial and temporal release of a therapeutic is one of the key challenges in biomedical research that can ultimately lead to society-wide improvement in disease management. In recent years, substrate mediated delivery of cargo has shown great promise in applications including drug and gene eluding films/scaffolds,[64-67] coatings for stents,[68, 69] and other implantable devices,[70, 71] and controlling stem cell differentiation.[72] Specifically, the drug delivery kinetics is particularly relevant when it is necessary to achieve effective dose and spatiotemporal release kinetics of the therapeutic agent at the intended site of injury. Delivery via immobilization of the therapeutic cargo to a solid platform demonstrates higher translatable success compared to delivery using the free “bolus” form by overcoming unfavorable burst kinetics, toxic offsite effects, and efficacy reduction due to systemic dilution. This cargo confinement mechanism to the substrate platform have been engineered via ionic[73], chemical[74] , and physical means[75, 76] to achieve controlled spatial organization, while cargo release has been catalyzed by changes in local pH, temperature, and material-intrinsic shifts (ex. swelling and hydrolysis driven degradation) to acquire specific temporal release profiles.[77] Although considerable progress has been made, there is a lack in the development of a substrate-mediated delivery system capable of simultaneous controlled and truly localized delivery of therapeutics.

## 5.3. Lipid Nanoparticle Biodistribution Analysis *in vivo* as a function of HA Length

In 2015 nearly 1,600 deaths will occur daily in the US as a result of cancer or cancer related complications, and over 1,665,540 Americans will be diagnosed with invasive cancer [44]. Depending on the specific type/ stage of cancer, traditional treatment options include chemotherapy, radiation therapy, hormone therapy, and biological therapy [44, 78]. These treatment measures are invasive, induce an array of adverse side effects, or only work until the body develops a specific resistance. The use of advanced drug delivery systems (ADDS) to transport chemotherapeutics specifically to cancer cells preferentially over normal cells is a relatively new treatment option for cancer patients, and has yielded massive attention and subsequent capital and intellectual investment. The ability for an ADDS to transport cargo with variable solubility and unfavorable pharmacokinetics while exhibiting cargo protection, controlled release, and targeting capabilities is the ultimate goal in order to decrease variability in systemic concentration and therefore require less overall dosage during treatment [78, 79]. By definition, drug delivery systems are engineered technologies such as nanoparticles, virus-based nanocarriers, etc. created to aid and mediate the delivery of a therapeutic agent [79]. ADDS utilize targeted delivery mechanisms to deliver cargo to specific coordinates of the body by either a passive process such as the Enhanced Permeability and Retention effect (EPR) exhibited in tumors due to leaky vasculature, or an active process such as specific ligand interactions. Since their discovery in the 1960s, lipid based nanoparticles (LNPs) have been at the forefront of drug delivery due to their biocompatibility, modifiable surface characteristics, and ease of creation [21]. Surface crosslinking of LNPs with

extracellular matrix (ECM) proteins such as Hyaluronic Acid has been shown to provide a hydrophilic barrier against opsonization *in vivo*, while also exhibiting dual functionality as a targeting moiety for selective active transport [28, 30].

Hyaluronic Acid (HA) is a main component of the ECM whose molecular weight (MW) has been shown to dictate its function and overall role *in vivo*: low MW HA plays a role in cellular signaling and is known to stimulate angiogenesis and the innate immune response, while high MW HA plays a structural role for cells and is known to be relatively inert in cell signaling [80]. For ADDS applications, HA has begun to draw attention for its ability to specifically bind and promote endocytosis inside various cancer cells that overexpress CD44 surface receptor [81]. CD44 is a glycoprotein receptor that is involved in pathological conditions including tumor growth/ metastasis, and has been shown to increase in cell surface expression during the progression of oncogenesis, yielding a preferential binding domain for HA conjugated LNPs [82]. Both *in vitro* and *in vivo* models have validated that the affinity of the interaction between HA and CD44 directly correlates to the MW of the HA polymer [13, 83]. However, a current lack in the understanding of how the MW and surface coating density of HA on LNP surfaces affects uptake and accumulation in the liver during systemic administration *in vivo* is hindering progress in the usage of such conjugate LNP platforms. The interaction between the HA- LNPs and both the Kupffer cells (KCs) and Liver Sinusoidal Endothelial Cells (LSECs) of the liver needs to be probed to determine optimum conditions for systemic delivery to reduce hepatotoxicity and increase accumulation in the target tumor site. This research will lead to an improved strategy to deliver cargo

including chemotherapeutics, silencing RNA, DNA, etc. for the treatment of a variety of cancer models.

# References


1. Zhang, L., et al., *Nanoparticles in Medicine: Therapeutic Applications and Developments.* Clinical Pharmacology & Therapeutics, 2008. **83**(5): p. 761-769.
2. Moghimi, S.M., A.C. Hunter, and J.C. Murray, *Nanomedicine: current status and future prospects.* The FASEB Journal, 2005. **19**(3): p. 311-330.
3. Rana, S., et al., *Monolayer coated gold nanoparticles for delivery applications.* Advanced Drug Delivery Reviews, 2012. **64**(2): p. 200-216.
4. Patel, N. and S. Panda, *Liposome drug delivery system: a critic review.* Journal of pharmaceutical science and bioscientic resaearch, 2012. **2**(4): p. 162-194.
5. Elzoghby, A.O., W.M. Samy, and N.A. Elgindy, *Protein-based nanocarriers as promising drug and gene delivery systems.* Journal of Controlled Release, 2012. **161**(1): p. 38-49.
6. Bangham, A.D., *Surrogate cells or Trojan horses. The discovery of liposomes.* Bioessays, 1995. **17**(12): p. 1081-8.
7. Bangham, J.A. and E.J.A. Lea, *The Interaction of detergernts with bilayer lipid membranes.* Biochima et Biophysica Acta, 1978. **511**(3).
8. Bangham, A., M. Hill, and N. Miller, *Preparation and use of liposomes as models of biological membranes*. 1974: Springer.
9. Israelachvili, J.N., D.J. Mitchell, and B.W. Ninham, *Theory of self-assembly of hydrocarbon amphiphiles into micelles and bilayers.* Journal of the Chemical Society, Faraday Transactions 2: Molecular and Chemical Physics, 1976. **72**: p. 1525-1568.

10. Dua, J., A. Rana, and A. Bhandari, *Liposome: methods of preparation and applications.*

11. Immordino, M.L., F. Dosio, and L. Cattel, *Stealth Liposomes review of the basic science, rationale, and clinical applications, existing and potential.* International Journal of Nanomedicine, 2006. **3**: p. 297-315.

12. Leonor Pinzon-Daza, M., et al., *Nanoparticle-and liposome-carried drugs: new strategies for active targeting and drug delivery across blood-brain barrier.* Current drug metabolism, 2013. **14**(6): p. 625-640.

13. Mizrahy, S., et al., *Hyaluronan-coated nanoparticles: the influence of the molecular weight on CD44-hyaluronan interactions and on the immune response.* J Control Release, 2011. **156**(2): p. 231-8.

14. Peer, D. and R. Margalit, *Tumor-targeted hyaluronan nanoliposomes increase the antitumor activity of liposomal Doxorubicin in syngeneic and human xenograft mouse tumor models.* Neoplasia, 2004. **6**(4): p. 343-53.

15. Noble, G.T., et al., *Ligand-targeted liposome design: challenges and fundamental considerations.* Trends in Biotechnology. **32**(1): p. 32-45.

16. Kraft, J.C., et al., *Emerging Research and Clinical Development Trends of Liposome and Lipid Nanoparticle Drug Delivery Systems.* Journal of Pharmaceutical Sciences, 2014. **103**(1): p. 29-52.

17. Meunier, F., H.G. Prentice, and O. Ringden, *Liposomal amphotericin B (AmBisome): safety data from a phase II/III clinical trial.* J Antimicrob Chemother, 1991. **28 Suppl B**: p. 83-91.

18. Stegmann, T., et al., *Functional reconstitution of influenza virus envelopes.* Embo j, 1987. **6**(9): p. 2651-9.

19. Allen, T.M. and P.R. Cullis, *Liposomal drug delivery systems: from concept to clinical applications.* Advanced drug delivery reviews, 2013. **65**(1): p. 36-48.

20. Allen, T.M. and P.R. Cullis, *Drug delivery systems: entering the mainstream.* Science, 2004. **303**(5665): p. 1818-1822.

21. Akbarzadeh, A., et al., *Liposome: classification, preparation, and applications.* Nanoscale Res Lett, 2013. **8**(1): p. 102.

22. Li, X., et al., *Doxorubicin physical state in solution and inside liposomes loaded via a pH gradient.* Biochimica et Biophysica Acta (BBA)-Biomembranes, 1998. **1415**(1): p. 23-40.

23. Modi, S., T.-X. Xiang, and B.D. Anderson, *Enhanced active liposomal loading of a poorly soluble ionizable drug using supersaturated drug solutions.* Journal of Controlled Release, 2012. **162**(2): p. 330-339.

24. Arshinova, O., et al., *Drug Synthesis Methods and Manufacutring Technology: Lyophilization of Liposomal Drug Dorms (review).* Pharmaceutical Chemistry Journal, 2011. **46**(4).

25. Chen, C., et al., *An overview of liposome lyophilization and its future potential.* J Control Release, 2010. **142**(3): p. 299-311.

26. Henry-Michellang, S., et al., *Lyophilization and Rehydration of Liposomes.* Colloids and Surfaces, 1984. **14**(3-4).

27. Peer, D. and R. Margalit, *Physicochemical evaluation of a stability-driven approach to drug entrapment in regular and in surface-modified liposomes.* Arch Biochem Biophys, 2000. **383**(2): p. 185-90.

28. Peer, D., et al., *Systemic leukocyte-directed siRNA delivery revealing cyclin D1 as an anti-inflammatory target.* Science, 2008. **319**(5863): p. 627-30.

29. Chaudhury, A., et al., *Lyophilization of cholesterol-free PEGylated liposomes and its impact on drug loading by passive equilibration.* Int J Pharm, 2012. **430**(1-2): p. 167-75.

30. Peer, D. and R. Margalit, *Loading mitomycin C inside long circulating hyaluronan targeted nano-liposomes increases its antitumor activity in three mice tumor models.* Int J Cancer, 2004. **108**(5): p. 780-9.

31. Srinivasan, C., D. Peer, and M. Shimaoka, *Integrin-targeted stabilized nanoparticles for an efficient delivery of siRNAs in vitro and in vivo.* Methods Mol Biol, 2012. **820**: p. 105-16.

32. Margalit, R., et al., *Liposomal drug delivery: thermodynamics and chemical kinetic considerations.* Journal of Controlled Release, 1991. **17**(3): p. 285-296.

33. Margalit, R., et al., *Bioadhesive liposomes as topical drug delivery systems molecular and cellular studies.* Journal of Controlled Release, 1992. **19**: p. 275-288.

34. Gregoriadis, G., *Liposomes as drug carriers : recent trends and progress*. 1988, Chichester [etc.]: Wiley.

35. Peer, D., A. Florentin, and R. Margalit, *Hyaluronan is a key component in cryoprotection and formulation of targeted unilamellar liposomes.* Biochimica et Biophysica Acta (BBA) - Biomembranes, 2003. **1612**(1): p. 76-82.

36. Heurtault, B., et al., *Physico-chemical stability of colloidal lipid particles.* Biomaterials, 2003. **24**(23): p. 4283-4300.

37. PANYAM, J., et al., *Rapid endo-lysosomal escape of poly(dl-lactide-co-glycolide) nanoparticles: implications for drug and gene delivery.* The FASEB Journal, 2002. **16**(10): p. 1217-1226.

38. Iversen, T.-G., T. Skotland, and K. Sandvig, *Endocytosis and intracellular transport of nanoparticles: present knowledge and need for future studies.* Nano Today, 2011. **6**(2): p. 176-185.

39. Witting, M., et al., *Recent advances in topical delivery of proteins and peptides mediated by soft matter nanocarriers.* Biotechnology Advances, (0).

40. Draghici, B. and M.A. Ilies, *Synthetic nucleic acid delivery systems: present and perspectives.* Journal of medicinal chemistry, 2015.

41. Cruje, C. and D. Chithrani, *Polyethylene Glycol Density and Length Affects Nanoparticle Uptake by Cancer Cells.* J Nanomed Res, 2014. **1**(1): p. 00006.

42. Band, V., et al., *Tumor progression in four mammary epithelial cell lines derived from the same patient.* Cancer Res, 1990. **50**(22): p. 7351-7.

43. Go, A.S., et al., *Heart disease and stroke statistics--2014 update: a report from the American Heart Association.* Circulation, 2014. **129**(3): p. e28.

44. *Cancer Facts and Figures 2015.* American Cancer Society, 2015(Atlanta: American Cancer Society).

45. Stupp, R., K. Homicsko, and J.G. Cairncross, *Malignant Glioma: Viewpoint—Chemotherapy*, in *Principles and Practice of Stereotactic Radiosurgery*. 2015, Springer. p. 279-293.

46. Alvarez-Erviti, L., et al., *Delivery of siRNA to the mouse brain by systemic injection of targeted exosomes.* Nature biotechnology, 2011. **29**(4): p. 341-345.

47. Alcaraz, J. and P. Roca-Cusachs, *Shape and Mechanical Cues Underlying Cellular Homeostasis in Soft Organs.* Cells, Forces, and the Microenvironment, 2015: p. 177.

48. Plodinec, M., et al., *The nanomechanical signature of breast cancer.* Nat Nano, 2012. **7**(11): p. 757-765.

49. Bufi, E., et al., *Role of the apparent diffusion coefficient in the prediction of response to neoadjuvant chemotherapy in patients with locally advanced breast cancer.* Clinical Breast Cancer, 2015.

50. Tannock, I.F., *Tumor physiology and drug resistance.* Cancer and Metastasis Reviews, 2001. **20**(1-2): p. 123-132.

51. Lu, P., V.M. Weaver, and Z. Werb, *The extracellular matrix: a dynamic niche in cancer progression.* The Journal of cell biology, 2012. **196**(4): p. 395-406.

52. Ingber, D.E. *Can cancer be reversed by engineering the tumor microenvironment?* in *Seminars in cancer biology*. 2008. Elsevier.

53. Manzoor, A.A., et al., *Overcoming limitations in nanoparticle drug delivery: triggered, intravascular release to improve drug penetration into tumors.* Cancer research, 2012. **72**(21): p. 5566-5575.

54. Brannon-Peppas, L. and J.O. Blanchette, *Nanoparticle and targeted systems for cancer therapy.* Advanced drug delivery reviews, 2012. **64**: p. 206-212.

55. Palchesko, R.N., et al., *Development of Polydimethylsiloxane Substrates with Tunable Elastic Modulus to Study Cell Mechanobiology in Muscle and Nerve.* PLoS ONE, 2012. **7**(12): p. 1-13.

56. Samani, A., J. Zubovits, and D. Plewes, *Elastic moduli of normal and pathological human breast tissues: an inversion-technique-based investigation of 169 samples.* Physics in medicine and biology, 2007. **52**(6): p. 1565.

57. Souter, L.H., et al., *Human 21T breast epithelial cell lines mimic breast cancer progression in vivo and in vitro and show stage-specific gene expression patterns.* Lab Invest, 2010. **90**(8): p. 1247-1258.

58. Bhana, B., et al., *Influence of substrate stiffness on the phenotype of heart cells.* Biotechnology and bioengineering, 2010. **105**(6): p. 1148-1160.

59. Huang, C., et al., *Substrate stiffness regulates cellular uptake of nanoparticles.* Nano letters, 2013. **13**(4): p. 1611-1615.

60. Lasic, D.D., *Novel applications of liposomes.* Trends Biotechnol, 1998. **16**(7): p. 307-21.

61. Burgess, P., et al., *On firm ground: IP protection of therapeutic nanoparticles.* Nat Biotech, 2010. **28**(12): p. 1267-1270.

62. Chang, H.I. and M.K. Yeh, *Clinical development of liposome-based drugs: formulation, characterization, and therapeutic efficacy.* Int J Nanomedicine, 2012. **7**: p. 49-60.

63. Peer, D., et al., *Systemic Leukocyte-Directed siRNA Delivery Revelaing Cyclin D1 as an Anti-Inflammatory Target.* Science, 2008. **319**: p. 627-630.

64. Chen, D., et al., *Robust and flexible free-standing films for unidirectional drug delivery.* Langmuir, 2013. **29**(26): p. 8328-8334.

65. Huang, C.L., W.L. Lee, and J.S.C. Loo, *Drug-eluting scaffolds for bone and cartilage regeneration.* Drug Discovery Today, 2014. **19**(6): p. 714-724.

66. Ji, W., et al., *Bioactive electrospun scaffolds delivering growth factors and genes for tissue engineering applications.* Pharmaceutical research, 2011. **28**(6): p. 1259-1272.

67. Garg, T., et al., *Scaffold: a novel carrier for cell and drug delivery.* Critical Reviews™ in Therapeutic Drug Carrier Systems, 2012. **29**(1).

68. Kang, S.-H., et al., *Biodegradable-polymer drug-eluting stents vs. bare metal stents vs. durable-polymer drug-eluting stents: a systematic review and Bayesian approach network meta-analysis.* European heart journal, 2014: p. eht570.

69. Puranik, A.S., E.R. Dawson, and N.A. Peppas, *Recent advances in drug eluting stents.* International journal of pharmaceutics, 2013. **441**(1): p. 665-679.

70. Kleiner, L.W., J.C. Wright, and Y. Wang, *Evolution of implantable and insertable drug delivery systems.* Journal of Controlled Release, 2014. **181**: p. 1-10.

71. Glauser, T., I. Astafieva, and S.F.A. Hossainy, *Coatings for implantable medical devices for controlled release of a hydrophilic drug and a hydrophobic drug*. 2014, Google Patents.

72. Brunger, J.M., et al., *Scaffold-mediated lentiviral transduction for functional tissue engineering of cartilage.* Proceedings of the National Academy of Sciences, 2014. **111**(9): p. E798-E806.

73. Volodkin, D., R. Von Klitzing, and H. Moehwald, *Polyelectrolyte Multilayers: Towards Single Cell Studies.* Polymers, 2014. **6**(5): p. 1502-1527.

74. Costa, F., et al., *Covalent immobilization of antimicrobial peptides (AMPs) onto biomaterial surfaces.* Acta Biomaterialia, 2011. **7**(4): p. 1431-1440.

75. Vashist, A., et al., *Recent advances in hydrogel based drug delivery systems for the human body.* Journal of Materials Chemistry B, 2014. **2**(2): p. 147-166.

76. Dhandayuthapani, B., et al., *Polymeric scaffolds in tissue engineering application: a review.* International Journal of Polymer Science, 2011. **2011**.

77. Zelikin, A.N., *Drug releasing polymer thin films: new era of surface-mediated drug delivery.* Acs Nano, 2010. **4**(5): p. 2494-2509.

78. Robinson, D. and J.W. Mauger, *Drug delivery systems.* American Journal of Health-System Pharmacy, 1991. **48**(10 Suppl): p. S14-S23.

79. De Jong, W.H. and P.J. Borm, *Drug delivery and nanoparticles: applications and hazards.* International journal of nanomedicine, 2008. **3**(2): p. 133.

80. Arpicco, S., G. De Rosa, and E. Fattal, *Lipid-Based Nanovectors for Targeting of CD44-Overexpressing Tumor Cells.* J Drug Deliv, 2013. **2013**: p. 860780.

81. Choi, K.Y., et al., *Hyaluronic acid-based nanocarriers for intracellular targeting: interfacial interactions with proteins in cancer.* Colloids Surf B Biointerfaces, 2012. **99**: p. 82-94.

82. Orian-Rousseau, V., *CD44, a therapeutic target for metastasising tumours.* European Journal of Cancer, 2010. **46**(7): p. 1271-1277.

83. Mizrahy, S., et al., *Tumor targeting profiling of hyaluronan-coated lipid based-nanoparticles.* Nanoscale, 2014. **6**(7): p. 3742-3752.